© 2019. Published by The Company of Biologists Ltd | Development (2019) 146, dev180430. doi:10.1242/dev.180430

RESEARCH ARTICLE

Lats1 and *Lats2* are required for the maintenance of multipotency in the Müllerian duct mesenchyme

Guillaume St-Jean[1], Mayra Tsoi[1], Atefeh Abedini[2], Adrien Levasseur[1], Charlène Rico[1], Martin Morin[3], Bojana Djordjevic[4], Ilkka Miinalainen[5], Riitta Kaarteenaho[6], Marilène Paquet[7], Nicolas Gévry[3], Alexandre Boyer[1], Barbara Vanderhyden[2] and Derek Boerboom[1,*]

ABSTRACT

WNT signaling plays essential roles in the development and function of the female reproductive tract. Although crosstalk with the Hippo pathway is a key regulator of WNT signaling, whether Hippo itself plays a role in female reproductive biology remains largely unknown. Here, we show that conditional deletion of the key Hippo kinases *Lats1* and *Lats2* in mouse Müllerian duct mesenchyme cells caused them to adopt the myofibroblast cell fate, resulting in profound reproductive tract developmental defects and sterility. Myofibroblast differentiation was attributed to increased YAP and TAZ expression (but not to altered WNT signaling), leading to the direct transcriptional upregulation of *Ctgf* and the activation of the myofibroblast genetic program. Müllerian duct mesenchyme cells also became myofibroblasts in male mutant embryos, which impeded the development of the male reproductive tract and resulted in cryptorchidism. The inactivation of *Lats1/2* in differentiated uterine stromal cells *in vitro* did not compromise their ability to decidualize, suggesting that Hippo is dispensable during implantation. We conclude that Hippo signaling is required to suppress the myofibroblast genetic program and maintain multipotency in Müllerian mesenchyme cells.

KEY WORDS: *Lats1/2*, Uterus, Müllerian duct, Mesenchyme, Myofibroblast, Cell fate, Mouse

INTRODUCTION

The Müllerian ducts (or paramesonephric ducts) are paired embryonic structures that give rise to most of the female reproductive tract. They comprise a luminal epithelial cell population, mesenchymal cells that surround the epithelium, and an outer coelomic epithelium. The ducts form when specialized cells from the rostral mesonephros invaginate and elongate caudally alongside the Wolffian ducts, until they join at the urogenital sinus. In male embryos, the production of anti-Müllerian hormone (AMH) causes the Müllerian ducts to degenerate, and testosterone spurs the development of the Wolffian duct into the male reproductive tract. In the female, absence of AMH allows the Müllerian ducts to further develop, fuse and differentiate into the oviducts, uterus and anterior vagina (Roly et al., 2018).

All steps of the initiation, invagination, elongation and differentiation (or degradation) of the Müllerian ducts is tightly coordinated by a number of signaling effectors and pathways. Among these, members of the WNT family of secreted glycoprotein signaling molecules play prominent roles. Using cell-fate mapping and neutralizing antibodies, WNT4 was shown to be required for Müllerian duct invagination and elongation (Prunskaite-Hyyrylainen et al., 2016), and *Wnt4* null mice are born without Müllerian structures (Vainio et al., 1999). Additional studies in mice using hypomorphic alleles and conditional targeting have shown that *Wnt4* is also involved in the development of the oviduct and the myometrium (Prunskaite-Hyyrylainen et al., 2016). *Wnt5a* null mice lack both cervix and vagina, and have short, coiled uterine horns (Mericskay et al., 2004). Moreover, deletion of the *Wnt7a* gene results in a partially posteriorized female reproductive tract, with uterus-like oviducts and a uterus with histological characteristics of the vagina (Dunlap et al., 2011). *Wnt4*, *Wnt5a* and *Wnt7a* have also all been implicated in uterine gland formation (Dunlap et al., 2011; Farah et al., 2017; Franco et al., 2011; Mericskay et al., 2004; St-Jean et al., 2019). Although the signaling processes whereby WNT ligands direct the development of the female reproductive tract are poorly understood, the canonical WNT signaling effector β-catenin (CTNNB1) is believed to play an important role, largely based on phenotypic abnormalities observed in *Ctnnb1* conditional knockout models that mimic to some extent those observed in knockout models of specific WNT genes (Deutscher and Hung-Chang Yao, 2007; Hernandez Gifford et al., 2009). How WNT signaling itself is regulated in the Müllerian duct and during reproductive tract development remains essentially unknown.

The Hippo signaling pathway plays important roles in the embryonic development of many tissues such as the heart (Heallen et al., 2011), nervous system (Bao et al., 2017) and kidneys (McNeill and Reginensi, 2017; Reginensi et al., 2016) by regulating cellular processes, including proliferation, apoptosis and differentiation. Hippo is not activated by a specific ligand, but rather responds to a multitude of extra- and intracellular cues such as cell-cell contact, cell polarity, mechanical forces and several G protein-coupled receptor ligands (Lv et al., 2015; Yu et al., 2012; Zhao et al., 2007). The pathway consists of a core kinase cascade that culminates in the activation of the kinases large tumor suppressor (LATS) 1 and 2. Once activated, LATS1/2 can phosphorylate the transcriptional co-regulatory molecules YAP (YAP1) and TAZ, resulting in their cytoplasmic sequestration and

[1]Département de Biomédecine Vétérinaire, Faculté de Médecine Vétérinaire, Université de Montréal, St-Hyacinthe, Québec, J2S 7C6, Canada. [2]Department of Cellular and Molecular Medicine, University of Ottawa, Ottawa, Ontario, K1H 8M5, Canada. [3]Département de Biologie, Faculté des Sciences, Université de Sherbrooke, Sherbrooke, Québec, J1K 2R1, Canada. [4]Department of Anatomic Pathology, Sunnybrook Health Sciences Centre, Toronto, Ontario, M4N 3M5, Canada. [5]Biocenter Oulu, University of Oulu, FI-90014 Oulu, Finland. [6]Research Unit of Internal Medicine, University of Oulu and Medical Research Center Oulu, Oulu University Hospital, 90029, Oulu, Finland. [7]Département de Pathologie et de Microbiologie, Faculté de Médecine Vétérinaire, Université de Montréal, St-Hyacinthe, Québec, J2S 7C6, Canada.

*Author for correspondence (derek.boerboom@umontreal.ca)

D.B., 0000-0003-4454-0589

Received 14 May 2019; Accepted 18 September 2019

Development (2019) 146, dev180430. doi:10.1242/dev.180430

degradation. Inactivation of the pathway results in the translocation of unphosphorylated YAP and TAZ to the nucleus, which bind to various transcription factors (including those of the TEAD family) to modulate the expression of specific target genes (Tsutsumi et al., 2013; Zhao et al., 2008). Importantly, recent studies have established functional interactions between Hippo and the canonical WNT signaling pathway. For instance, TAZ was found to inhibit WNT signaling by interacting with the WNT signaling effector Disheveled (Varelas et al., 2010). YAP/TAZ can also recruit the ubiquitin ligase β-TRCP (BTRC) to a multiprotein complex that directs the ubiquitylation and degradation of CTNNB1 (Azzolin et al., 2014). Furthermore, YAP and CTNNB1 can physically interact when in the nucleus and bound to their respective transcription factor partners, and this interaction enhances target gene transcriptional activity (Heallen et al., 2011). Although this mutual interdependence between Hippo and canonical WNT signaling has been shown in several cell types, whether or not this occurs within the Müllerian duct during reproductive tract development has never been reported.

A few recent studies have suggested that the Hippo pathway may also play important roles in postnatal uterine physiology and disease processes. For instance, Strakova et al. reported decreased expression of TAZ in the nuclei of human uterine fibroblasts during *in vitro* decidualization, as well as decreased TAZ expression in the uterine stroma during the secretory phase of the menstrual cycle, suggesting a potential role in decidualization and implantation (Strakova et al., 2010). Increased expression of both *YAP* (*YAP1*) and *TEAD1* mRNA levels has also been observed during decidualization in cultured human endometrial stromal cells. Knockdown of YAP in these cells delayed the morphological and gene expression changes associated with decidualization (Chen et al., 2017). Further studies have suggested roles for dysregulated YAP and/or TAZ in the pathogenesis of endometriosis (Song et al., 2016) and uterine cancers (Liu et al., 2013a; Zhan et al., 2016).

To determine the roles of Hippo signaling in the development and function of the female reproductive tract, we generated mouse models to inactivate *Lats1* and/or *Lats2* in Müllerian mesenchyme cells. Unexpectedly, loss of Hippo signaling caused the mesenchyme cells to lose their ability to differentiate into uterine and oviduct stromal and smooth cells. Rather, loss of *Lats1/2* directed the mesenchymal cells to adopt the myofibroblast fate, resulting in severe developmental defects of the uterus and absent oviducts. These effects were attributed to increased YAP and TAZ (but not CTNNB1) expression and transcriptional regulatory activity, leading to the activation of the myofibroblast genetic program. Together, our findings indicate a previously unsuspected role for the Hippo pathway in the maintenance of multipotency in Müllerian mesenchyme cells.

RESULTS

Loss of *Lats1* and *Lats2* results in multiple developmental defects of the Müllerian duct and female reproductive tract

To study the roles of the Hippo pathway in the development and physiology of the female reproductive tract, we first determined the expression of its key components. Immunohistochemical analyses showed weak TAZ expression throughout all stages of development compared with the other Hippo effectors. Staining was mostly absent in embryonic day (E) 17.5 and newborn mice, whereas weak cytoplasmic staining appeared in the endometrium and myometrium of adult mice (Fig. S1). Conversely, high levels of LATS1, LATS2 and YAP expression were found at all stages of development. Their expression localized mostly to the nucleus during early stages of development (E17.5 and newborn) in the Müllerian mesenchyme/uterine stroma, along with scant cytoplasmic signal in the luminal epithelium. In adult mice, LATS1, LATS2 and YAP nuclear and cytoplasmic expression was observed in all parts of the uterus (Fig. S1). PhosphoYAP expression mirrored that of YAP at E17.5, but was absent in the uteri of newborn mice. Cytoplasmic phosphoYAP expression then reappeared throughout the uterus in adult mice. (Fig. S1).

To inactivate Hippo signaling in the female reproductive tract, mice bearing floxed alleles for *Lats1* and/or *Lats2* were crossed with the *Amhr2*^{cre} strain, which targets the mesenchyme cells of the Müllerian duct, starting at the rostral end as early as E12.5 in mice of both sexes (Arango et al., 2008; Jamin et al., 2002). Whereas *Lats1*$^{flox/flox}$; *Amhr2*$^{cre/+}$ and *Lats2*$^{flox/flox}$; *Amhr2*$^{cre/+}$ females were fertile and had reproductive tracts that appeared normal at the gross and histological levels (not shown), *Lats1*$^{flox/flox}$; *Lats2*$^{flox/flox}$; *Amhr2*$^{cre/+}$ females were sterile (Table S1). Developmental time-course analyses of the reproductive tracts of *Lats1*$^{flox/flox}$; *Lats2*$^{flox/flox}$; *Amhr2*$^{cre/+}$ mice revealed numerous anomalies. Although no changes were apparent at E14.5 (not shown), by E17.5 the Müllerian duct was markedly thickened, with the presence of an abnormal cell population with an elongated, abundant, slightly eosinophilic cytoplasm and a plump nucleus. These appeared to replace most of the antimesometrial mesenchyme cell population (Fig. 1A). RT-qPCR analyses confirmed the loss of *Lats1* and *Lats2* expression in the Müllerian ducts of *Lats1*$^{flox/flox}$; *Lats2*$^{flox/flox}$; *Amhr2*$^{cre/+}$ mice, and immunohistochemical analyses showed that this loss of expression localized specifically to the ectopic cell population (Fig. S2). The changes in the Müllerian duct appeared to prevent it from elongating normally, resulting in coiling that could be seen macroscopically by E19.5 (Fig. 1B). *Lats1*$^{flox/flox}$; *Lats2*$^{flox/flox}$; *Amhr2*$^{cre/+}$ females were born with plump and shortened uterine horns (Fig. 1B), with the ectopic cell population now appearing more differentiated and occupying most of the axial and antimesometrial regions of the uterine horns (Fig. 1A). In juvenile and adult mice, there was a severe architectural disorganization of the uterine layers, with an absence of demarcation between the endometrium and myometrium. As a result of the coiling, multiple lumens were often visible in transverse sections, and glands were sparse or absent. Cystic structures were often present adjacent to the ovary in juvenile mice (Fig. 1B). These were lined with ciliated epithelial cells (Fig. 1B, 'P21' inset), and presumed to be severely dilated oviduct. These structures typically ruptured by adulthood, leaving tattered remains and no recognizable oviduct. The ovaries were connected to the uterine walls by bands of tissue consisting of disorganized fibroblasts and smooth muscle cells (Fig. 1B, 'Adult' inset).

Loss of Hippo signaling causes Müllerian mesenchyme cells to commit to the myofibroblast fate

To characterize the cellular changes observed in the Müllerian ducts of *Lats1*$^{flox/flox}$; *Lats2*$^{flox/flox}$; *Amhr2*$^{cre/+}$ mice, we assessed proliferation by 5-bromo-2′-deoxyuridine (BrdU) incorporation at E17.5. Interestingly, the ectopic cell population was found to be non-proliferative, in contrast to the adjacent mesenchyme cells and Müllerian and coelomic epithelial cells (Fig. 2A). RT-qPCR and immunohistochemical analyses also showed a reduction in expression of the pluripotency markers *Sox2*, *Nanog* and *Oct4* (*Pou5f1*) in the Müllerian ducts, which was due to their absence in the ectopic cell population (Fig. 2B). These cells also stained positive for vimentin and smooth muscle actin (α-SMA), and Picrosirius Red stain showed abundant collagen deposition in

Development (2019) 146, dev180430. doi:10.1242/dev.180430

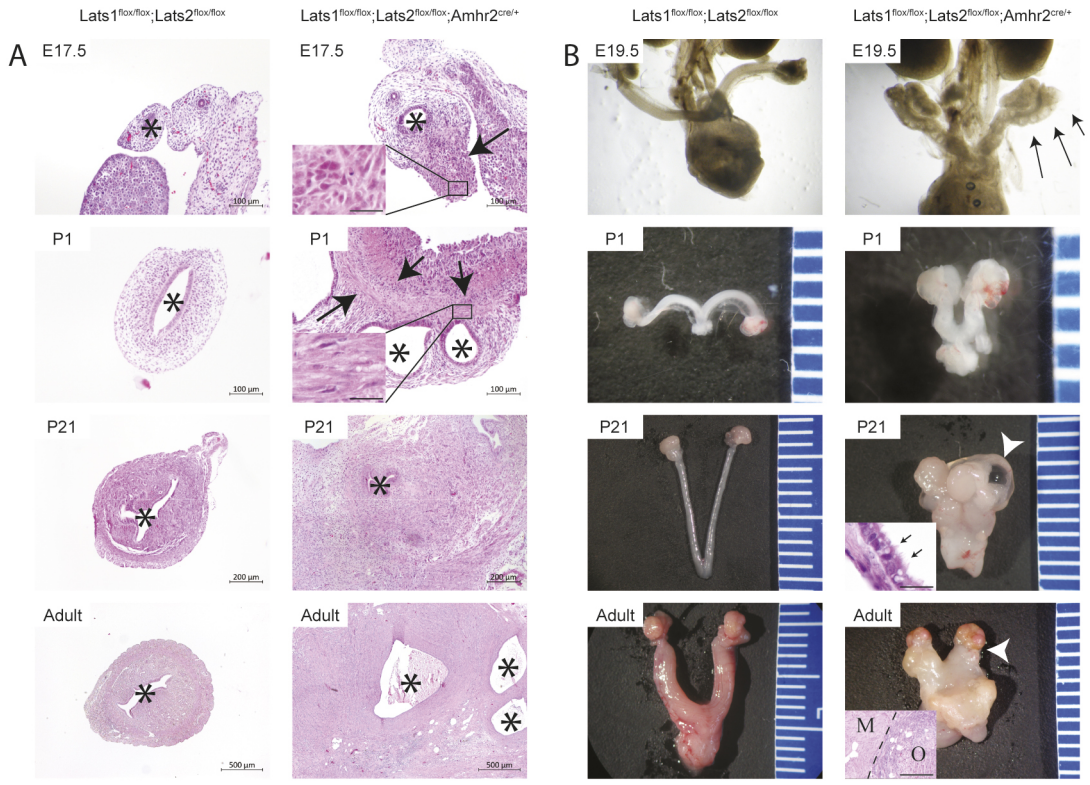

Fig. 1. Loss of Hippo signaling results in severe developmental defects of the female reproductive tract. (A) Representative photomicrographs of the reproductive tracts of E17.5, P1, P21 and adult female mice of the indicated genotypes stained with Hematoxylin-Eosin-Phloxine (HE). In E17.5 mutant mice, the antimesometrial portion of the Müllerian mesenchyme is replaced by abnormal cells with abundant, slightly eosinophilic cytoplasm (black arrow and inset). The abnormal cell population shows clear signs of differentiation in P1 mutant mice (black arrows and inset), unlike the control. P21 and adult mutant mice show loss of normal architecture of the uterine layers. Müllerian duct and uterine lumens are identified with asterisks. (B) Representative photographs of the dissected reproductive tracts of E19.5, P1, P21 and adult female mice of the indicated genotypes. E19.5 mutant mice showed abnormal elongation and coiling of the Müllerian ducts (black arrows). Dilation of oviduct is visible in P21 mutant mice (white arrowhead). Inset shows the dilated oviduct wall with the characteristic ciliated epithelium (black arrows). In adults, the oviduct is absent and the ovary is adhered directly to the uterine horn (white arrowhead and inset). M, myometrium/smooth muscle; O, ovary. Ruler graduations are in millimeters. Scale bars: 20 µm (P21 inset); 200 µm (Adult inset).

proximity to the ectopic cells, together strongly suggesting that they were myofibroblasts (Fig. 2C). This hypothesis was confirmed by transmission electron microscopy, which showed the presence of ultrastructural features, including thick intracellular actin belts and fibronexus junctions (Fig. 2D), that distinguish myofibroblasts from fibroblasts or smooth muscle cells (Eyden, 2008). Together, these findings indicate that loss of Hippo signaling in Müllerian mesenchyme cells causes them to lose their multipotency, while directing them to adopt the myofibroblast cell fate. In the uterus of adult *Lats1*$^{flox/flox}$; *Lats2*$^{flox/flox}$; *Amhr2*$^{cre/+}$ mice, the myofibroblasts were found interspersed between haphazard clusters of endometrial stromal cells and myometrial smooth muscle cells (Figs 1A and 2E).

Ovarian malformations in *Lats1*$^{flox/flox}$; *Lats2*$^{flox/flox}$; *Amhr2*$^{cre/+}$ mice

Ovaries from *Lats1*$^{flox/flox}$; *Lats2*$^{flox/flox}$; *Amhr2*$^{cre/+}$ mice were examined, as the *Amhr2*^{cre} allele also drives Cre expression in follicular granulosa cells and (to some extent) the ovarian stroma and surface epithelium (Arango et al., 2008; Baarends et al., 1994; Teixeira et al., 1996). In adult mice, a general reduction in the abundance of follicles was noted (Fig. 3). Corpora lutea were usually present, indicating that at least some follicles were able to develop fully, ovulate and luteinize. Some areas of cellular changes consistent with loss of granulosa cell differentiation were observed, as had been previously observed in the *Lats1*$^{flox/flox}$; *Lats2*$^{flox/flox}$; *CYP19*-cre model (Tsoi et al., 2019). In these areas, granulosa cells appeared to be replaced by large, round or polygonal cells with abundant, clear and slightly eosinophilic cytoplasm (Fig. 3, inset in image of mutant adult). The most striking change, however, was that most ovaries were partially covered by a thick layer of haphazardly organized, poorly differentiated elongated cells, suggestive of a neoplasm originating from the surface epithelium (Fig. 3). However, immunohistochemical analyses of ovarian cancer markers showed that these cells did not correspond to any known ovarian tumor type (Table S2, Fig. S3). Furthermore, they did not increase in number nor did they become invasive in older animals. A subsequent developmental time-course analysis showed that these cells in fact appeared to originate from the ovarian stroma. Morphological changes in the stroma were evident as early as E17.5 (Fig. 3), and seemed to develop into areas of exuberant overgrowth that extended past the ovarian surface, the growth of which appeared to be self-limiting.

Male reproductive tract defects in *Lats1*$^{flox/flox}$; *Lats2*$^{flox/flox}$; *Amhr2*$^{cre/+}$ mice

Developmental anomalies of the reproductive tract were also observed in male *Lats1*$^{flox/flox}$; *Lats2*$^{flox/flox}$; *Amhr2*$^{cre/+}$ mice. Rather than undergoing apoptosis during Müllerian duct regression (which is normally mostly completed around E15.5; Arango et al.,

Development (2019) 146, dev180430. doi:10.1242/dev.180430

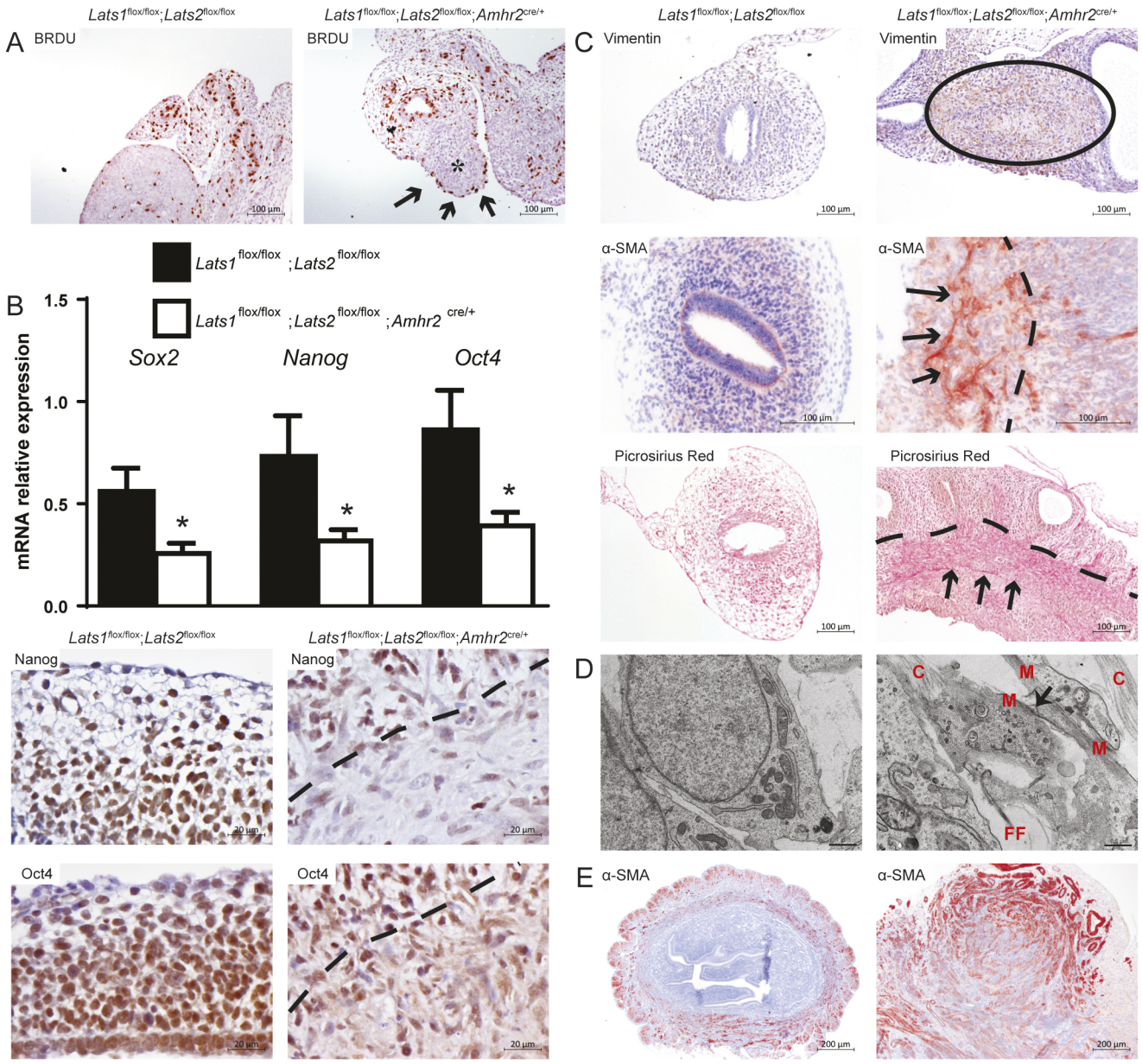

Fig. 2. Loss of Hippo signaling causes Müllerian mesenchyme cells to commit to the myofibroblast fate. (A) BrdU incorporation assays show proliferation in the coelomic epithelium (black arrows) in the vicinity of (but not within) the altered Müllerian mesenchyme (asterisk) in mutant mice at E17.5. (B) Graph shows RT-qPCR of pluripotency markers (*Sox2*, *Nanog*, *Oct4*) in the uteri of P1 mice of the indicated genotypes (n=6). Data are presented as mean±s.e.m. *P<0.05 (compared with controls), Student's t-test. Lower panels show immunohistochemistry analyses of NANOG and OCT4 in the same samples. Dashed line marks the boundary between normal (above) and abnormal (below) cell populations in the mutant group. (C) Immunohistochemistry analyses of vimentin and α-SMA expression in the uteri of P1 mice of the indicated genotypes. Note the positive signal within the abnormal cell population (black circle and black arrows). Picrosirius Red shows an abundance of collagen fibers (stained in red) in the altered tissues of the mutant group (black arrows). Dashed line marks the boundary between normal (above, left) and abnormal (below, right) cell populations. (D) Transmission electron microscopy analyses of uteri of P1 mice of the indicated genotypes. C, collagen bundle; F, extracellular fibril; M, peripheral myofilaments. Arrow indicates a fibronexus junction. Scale bars: 1 μm (control); 0.5 μm (mutant). (E) Immunohistochemistry analyses of α-SMA expression in the uteri of adult mice of the indicated genotypes.

2008), Müllerian mesenchyme cells persisted in *Lats1*$^{flox/flox}$; *Lats2*$^{flox/flox}$; *Amhr2*$^{cre/+}$ males and underwent changes similar to those observed in females. Histological analyses of E17.5 embryos showed the presence of Müllerian duct-derived myofibroblasts adjacent to the Wolffian ducts (Fig. 4A). These subsequently interfered with the elongation of the Wolffian ducts in a manner analogous to the Müllerian duct elongation defects observed in *Lats1*$^{flox/flox}$; *Lats2*$^{flox/flox}$; *Amhr2*$^{cre/+}$ females. As a result, newborn mice had thick and abnormally coiled epididymides and deferent ducts, with the head and body of the epididymis ectopically positioned at the cranial pole of the testis alongside the tail (Fig. 4A). The testes failed to descend in the mutant mice, resulting in pathological changes associated with cryptorchidism (e.g. testicular hypoplasia, atrophy, fibrosis, mineralization) in adults (Fig. 4B). Dilation of seminiferous tubules and of the epididymis (Fig. 4B) was also frequently observed in adult mice, suggesting that the developmental defects resulted in mechanical obstruction. Spermatozoa were rarely observed in the epididymis, and most

Development (2019) 146, dev180430. doi:10.1242/dev.180430

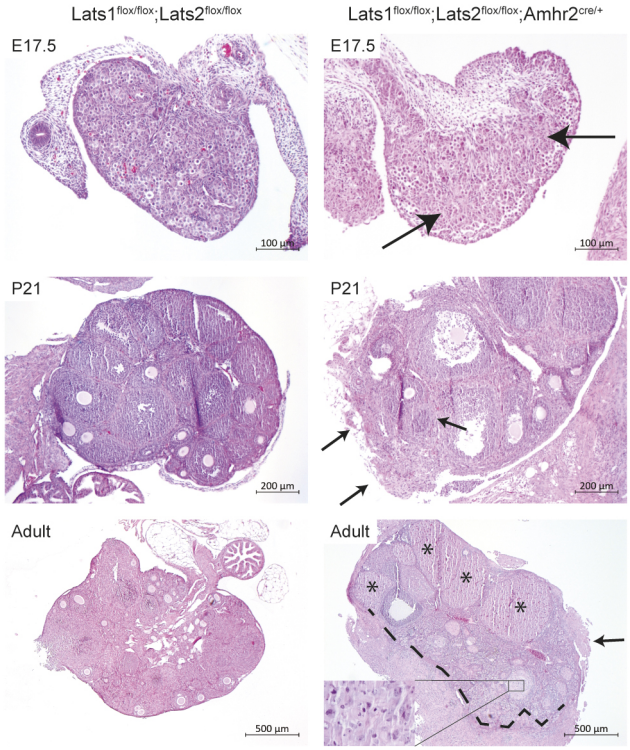

Fig. 3. Ovarian phenotypic changes in *Lats1*$^{flox/flox}$; *Lats2*$^{flox/flox}$; *Amhr2*$^{cre/+}$ mice. Photomicrographs of ovaries from E17.5, P21 and adult mice of the indicated genotypes Stained with Hematoxylin-Eosin-Phloxine (HE). In mutant mice, stromal changes were observed as early as E17.5 (black arrows) and expanded beyond the surface of the ovary at P21 (black arrows). In adult mutant mice, the ovary was covered by a cell population suggestive of an ovarian surface epithelium neoplasm (black arrow, delineated by dashed line). Loss of granulosa cell differentiation was observed within some follicles (inset). Corpora lutea are indicated with asterisks.

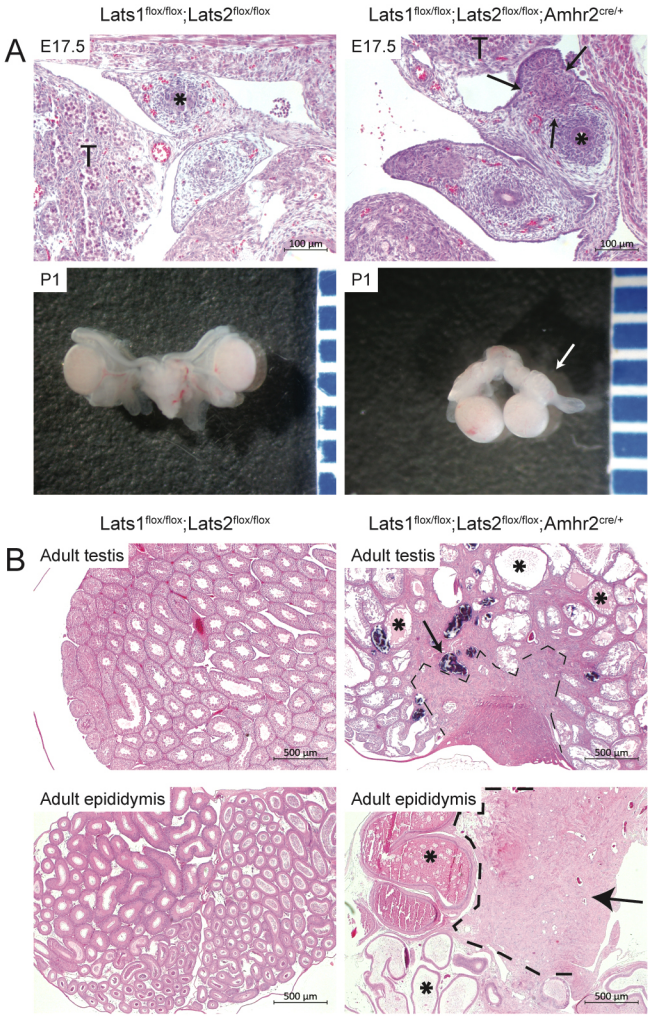

Fig. 4. Reproductive tract and testicular defects in male *Lats1*$^{flox/flox}$; *Lats2*$^{flox/flox}$; *Amhr2*$^{cre/+}$ mice. (A) Photomicrographs (E17.5) and photographs (P1) of reproductive tracts of mice of the indicated genotypes. Note the persistent Müllerian tissue (between black arrows) in the vicinity of the Wolffian duct (asterisk) in E17.5 mutant mice. T, testis. Photograph at P1 shows ectopically positioned epididymides and deferent ducts in mutant mice (white arrow). Ruler graduations are in millimeters. (B) Photomicrographs of testes and epididymides of adult mice of the indicated genotypes. Morphological changes associated with obstruction and cryptorchidism are evident in the testes of mutant mice. Seminiferous tubules are often dilated by eosinophilic material (cellular debris) (asterisks), degenerated and occasionally mineralized (black arrow). Foci of ectopic myofibroblasts are present in the mediastinum/rete testis (delineated by black dashed line) and within the epididymis of the mutant mice (delineated by black dashed line and black arrow), resulting in mechanical obstruction and dilation of the ducts (asterisk). Stain is Hematoxylin-Eosin-Phloxine (HE) in photomicrographs.

Lats1$^{flox/flox}$; *Lats2*$^{flox/flox}$; *Amhr2*$^{cre/+}$ males failed to sire litters in breeding trials.

Loss of *Lats1* and *Lats2* in endometrial stromal cells does not compromise their ability to undergo decidualization

As previous studies have suggested a role for the Hippo pathway in decidualization (Chen et al., 2017; Strakova et al., 2010), we investigated whether loss of *Lats1* and *Lats2* affects the ability of endometrial stromal cells to decidualize. As the uterine developmental defects in the *Lats1*$^{flox/flox}$; *Lats2*$^{flox/flox}$; *Amhr2*$^{cre/+}$ model precluded its use in conventional, *in vivo* decidualization assays, endometrial stromal cells from *Lats1*$^{flox/flox}$; *Lats2*$^{flox/flox}$ mice were placed in culture and infected with an adenovirus to drive Cre expression (Ad-Cre, to inactivate the floxed alleles) or an adenovirus that drives expression of eGFP (Ad-eGFP, control) for 24 h. Ad-Cre treatment resulted in ∼99% and ∼90% reduction of *Lats1* and *Lats2* mRNA levels, respectively (Fig. 5A). Following removal of the adenovirus, stromal cells were co-cultured with endometrial epithelial cells (separated by a semi-permeable membrane) and treated or not with medroxyprogesterone and cAMP to induce decidualization over a period of 48-72 h. Both the Ad-Cre- and Ad-eGFP-treated stromal cells responded to medroxyprogesterone+cAMP with a dramatic increase in decidual prolactin (*Prl8a2*) mRNA levels, indicating that decidualization occurred in both groups (Fig. 5A). Ad-Cre treatment did not change the mRNA levels of myofibroblast markers (Fig. 5B), indicating that loss of *Lats1/2* did not cause differentiated endometrial stromal cells to adopt myofibroblast characteristics. These results therefore suggest that Hippo signaling is dispensable for decidualization and cell fate maintenance in the uterine stroma.

Loss of *Lats1/2* causes a YAP/TAZ-driven induction of *Ctgf* and the myofibroblast genetic program

To elucidate the mechanism whereby loss of Hippo signaling causes Müllerian mesenchyme cells to commit to the myofibroblast cell fate, we first examined CTNNB1 expression in the uteri of newborn *Lats1*$^{flox/flox}$; *Lats2*$^{flox/flox}$; *Amhr2*$^{cre/+}$ mice. Although loss of *Lats1/2* was predicted to result in the hypophosphorylation and stabilization

Development (2019) 146, dev180430. doi:10.1242/dev.180430

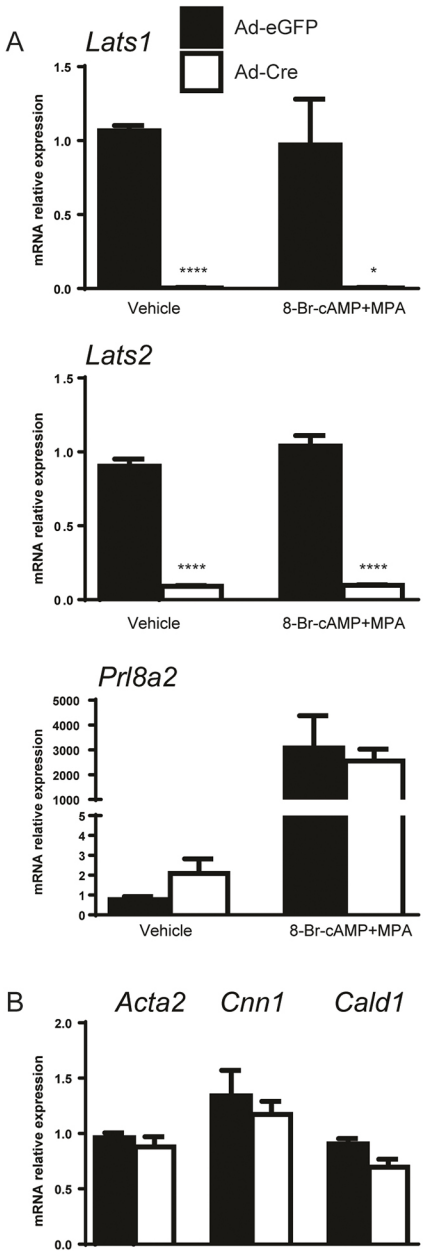

Fig. 5. Loss of Hippo signaling does not alter decidualization or cell fate in adult endometrial stromal cells. (A) RT-qPCR analysis of *Lats1*, *Lats2* and decidual prolactin (*Prl8a2*) mRNA levels in cultured uterine endometrial stromal cells from *Lats1*$^{flox/flox}$; *Lats2*$^{flox/flox}$ mice following 24 h treatment with Ad-Cre or Ad-eGFP, and 3 days of co-culture with epithelial cells and treatment with cAMP+medroxyprogesterone (or vehicle control). (B) mRNA levels of myofibroblast/muscle markers in samples similar to those shown in A, but omitting co-culture with epithelial cells. Data presented are mean±s.e.m. **P*<0.05, *****P*<0.0001 (compared with controls, analyzed by Student's *t*-test, *n*=3).

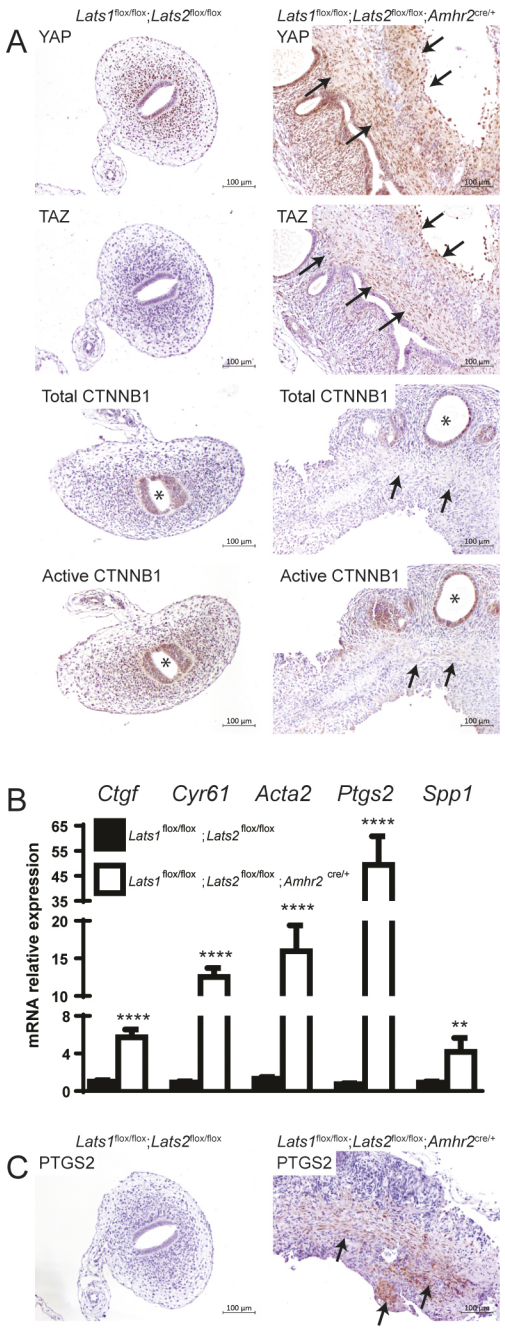

Fig. 6. YAP/TAZ-dependent induction of Hippo target genes and the myofibroblast genetic program in female *Lats1*$^{flox/flox}$; *Lats2*$^{flox/flox}$; *Amhr2*$^{cre/+}$ mice. (A) Immunohistochemistry analyses of YAP, TAZ, total CTNNB1 and active CTNNB1 expression in uteri of P1 mice of the indicated genotypes. For YAP and TAZ, arrows indicate increased cytoplasmic and nuclear staining in the ectopic myofibroblast cell population in mutant mice. For total CTNNB1 and active CTNNB1, arrows indicate low expression in the ectopic myofibroblast cell population. Asterisks indicate uterine lumen. (B) RT-qPCR analyses of Hippo pathway target genes (*Ctgf*, *Cyr61* at P1) and myofibroblast-associated genes (*Acta2*, *Ptgs2*, *Spp1* at E17.5). Data are mean±s.e.m. ***P*<0.01, *****P*<0.0001 (compared with controls, Student's *t*-test, *n*=6/genotype). (C) Immunohistochemistry analyses of PTGS2 expression in the Müllerian ducts of E17.5 mice of the indicated genotypes. Staining was limited to the ectopic myofibroblast cell population in mutant mice (black arrows).

of CTNNB1 (Varelas et al., 2010), both activated (i.e. unphosphorylated) and total CTNNB1 levels were in fact decreased in *Lats1*$^{flox/flox}$; *Lats2*$^{flox/flox}$; *Amhr2*$^{cre/+}$ myofibroblasts relative to control Müllerian mesenchyme and endometrial stromal cells (Fig. 6A). Conversely, YAP and TAZ levels were markedly increased in the mutant myofibroblasts. RT-qPCR analyses of uteri from *Lats1*$^{flox/flox}$; *Lats2*$^{flox/flox}$; *Amhr2*$^{cre/+}$ mice showed a strong and significant increase in the mRNA levels of the well-established YAP/TAZ target genes *Ctgf* (*Ccn2*; ∼6-fold) and *Cyr61* (*Ccn1*; ∼12-fold) relative to controls (Fig. 6B). Together, these results indicate that the loss of *Lats1/2* resulted in inactivation of the canonical Hippo

Development (2019) 146, dev180430. doi:10.1242/dev.180430

pathway in the *Lats1*$^{flox/flox}$; *Lats2*$^{flox/flox}$; *Amhr2*$^{cre/+}$ model, but did not induce CTNNB1 signaling.

To further determine how the loss of Hippo signaling affected the transcriptome in the Müllerian mesenchyme, ducts from E17.5 *Lats1*$^{flox/flox}$; *Lats2*$^{flox/flox}$; *Amhr2*$^{cre/+}$ and control mice were analyzed by microarray. These analyses identified 716 genes that were differentially expressed between genotypes by 2-fold or more. Of these, genes that were upregulated in the Müllerian ducts of *Lats1*$^{flox/flox}$; *Lats2*$^{flox/flox}$; *Amhr2*$^{cre/+}$ mice (n=547) were subjected to gene ontology analysis using the Metascape gene annotation and analysis resource. This showed that the upregulated genes regulate biological processes including blood vessel morphogenesis, the inflammatory response, extracellular matrix organization, wound healing and actin filament-based processes (Fig. S3), all of which are associated with myofibroblast functions (Klingberg et al., 2013; Gerarduzzi and Di Battista, 2017). Furthermore, six out of the 20 most highly upregulated genes have been associated with myofibroblast activation, differentiation or function (Table 1, genes in bold) (Elbjeirami et al., 2010; Garrett et al., 2004; Gomez et al., 2016; Lenga et al., 2008; Lipson et al., 2012; Mifflin et al., 2002; Nightingale et al., 2004; Sobral et al., 2011). RT-qPCR analyses were performed for selected genes to confirm the microarray analyses (Fig. 6B), and the most highly upregulated gene (*Ptgs2*) was evaluated by immunohistochemistry, which localized its expression to the myofibroblast cell population of newborn *Lats1*$^{flox/flox}$; *Lats2*$^{flox/flox}$; *Amhr2*$^{cre/+}$ mice, and confirmed its absence in controls (Fig. 6C). Genes that were downregulated in the Müllerian ducts of *Lats1*$^{flox/flox}$; *Lats2*$^{flox/flox}$; *Amhr2*$^{cre/+}$ mice were fewer in number (n=169) and were associated with biological processes including reproductive structure development and developmental growth (Fig. S4). The most downregulated gene identified in the microarray analysis was *Amhr2* (Table 2), the expression of which is normally restricted within the Müllerian duct to the mesenchyme cells (Arango et al., 2008). These results support the notion that loss of *Lats1/2* results in activation of the myofibroblast genetic program, while shutting off that of the Müllerian mesenchyme cells.

Table 1. Top 20 upregulated genes in *Lats1*$^{flox/flox}$; *Lats2*$^{flox/flox}$; *Amhr2*$^{cre/+}$ female mice

Gene	Fold change	*P*-value
Ptgs2	151.81	1.87E−09
Tac2	50.41	5.32E−08
Spp1	43.74	1.22E−07
Serpinb7	33.18	7.12E−08
Cyr61	20.48	3.79E−08
Slc2a3	19.62	3.08E−09
Inhba	18.84	7.24E−10
Osmr	18.59	5.34E−08
Ccl12	16.21	2.27E−07
Tnfrsf12a	15.39	1.36E−08
Rcan2	15.38	5.15E−08
Lcn2	15.34	0.0240
Bhlhe40	14.91	7.18E−09
Bmp4	14.19	6.90E−07
Gadd45g	14.12	2.56E−08
Plaur	12.68	3.12E−09
Ankrd1	12.6	3.26E−06
Ctgf	12.14	2.51E−08
Gpr50	11.89	0.0001
Fam180a	10.9	6.90E−07

Genes associated with myofibroblast activation, differentiation or function are in bold.

Table 2. Top 20 downregulated genes in *Lats1*$^{flox/flox}$; *Lats2*$^{flox/flox}$; *Amhr2*$^{cre/+}$ female mice

Gene	Fold change	*P*-value
Amhr2	−14.29	9.07E−08
Robo2	−7.71	7.94E−06
Gria1	−7.33	2.82E−07
Retnlg	−7.02	2.59E−07
Gstm7	−6.77	0.0007
Prdm1	−5.78	0.0004
Vsnl1	−5.68	0.0020
Gdpd3	−5.11	0.0003
Nr3c2	−4.7	5.94E−06
Stfa2	−4.7	0.0008
Synpo2	−4.59	2.13E−05
Mybpc1	−4.34	4.26E−05
Gm9912	−3.9	0.0001
Tex15	−3.77	6.00E−06
Epha6	−3.71	0.0345
Enpp2	−3.7	7.99E−06
Tcf24	−3.69	0.0485
Stfa2l1	−3.68	0.0015
Slc14a1	−3.51	0.0011
Plekhs1	−3.48	0.0029

To determine how YAP and TAZ may activate the myofibroblast genetic program, we examined their physical association with the promoter of *Ctgf*, a gene with established roles in myofibroblast differentiation and activation, and which is overexpressed in the *Lats1*$^{flox/flox}$; *Lats2*$^{flox/flox}$; *Amhr2*$^{cre/+}$ model (Fig. 6B, Table 1). Chromatin immunoprecipitation analyses showed enhanced binding of YAP to the *Ctgf* promoter in the uteri of *Lats1*$^{flox/flox}$; *Lats2*$^{flox/flox}$; *Amhr2*$^{cre/+}$ mice relative to controls, within ∼100 bp from the transcriptional start site, in an area that encompasses three consensus TEAD binding motifs (Fig. 7, top). A much more marked enhancement (∼10-fold) was obtained for TAZ in the same region of the promoter (Fig. 7, bottom). These data indicate that YAP/TAZ induce *Ctgf* transcription through direct binding of its promoter, and that TAZ may play a preponderant role in the induction of *Ctgf* expression in the *Lats1*$^{flox/flox}$; *Lats2*$^{flox/flox}$; *Amhr2*$^{cre/+}$ model.

DISCUSSION

Lats1 and *Lats2* are determinants of Müllerian mesenchyme cell fate

Several reports have shown that the Hippo pathway can act in pluripotent cell types to direct cell fate specification. For instance, during early embryonic development, Hippo signaling must be differentially regulated in the inner and outer cells of the morula to permit proper adoption of either the inner cell mass or trophectoderm cell fate (Sasaki, 2017). In the optic vesicle, YAP and TAZ cause pluripotent progenitor cells to adopt the retinal pigment epithelial cell fate (Miesfeld et al., 2015). In the liver, YAP/TAZ expression and activity determine whether hepatoblasts/progenitor cells become either hepatocytes or cholangiocytes (Lee et al., 2016; Nguyen et al., 2015). Likewise, Hippo signaling also appears to direct progenitor cells to give rise either to nephron epithelial cells or myofibroblasts in the developing kidney (McNeill and Reginensi, 2017). In this article, we show that Hippo signaling plays a similar role in Müllerian mesenchyme cells. Indeed, loss of Hippo activity in *Lats1*$^{flox/flox}$; *Lats2*$^{flox/flox}$; *Amhr2*$^{cre/+}$ mice caused Müllerian mesenchyme cells to cease proliferating, and adopt morphological, functional and gene expression characteristics of myofibroblasts. Simultaneously, these cells lost the expression of markers of

Development (2019) 146, dev180430. doi:10.1242/dev.180430

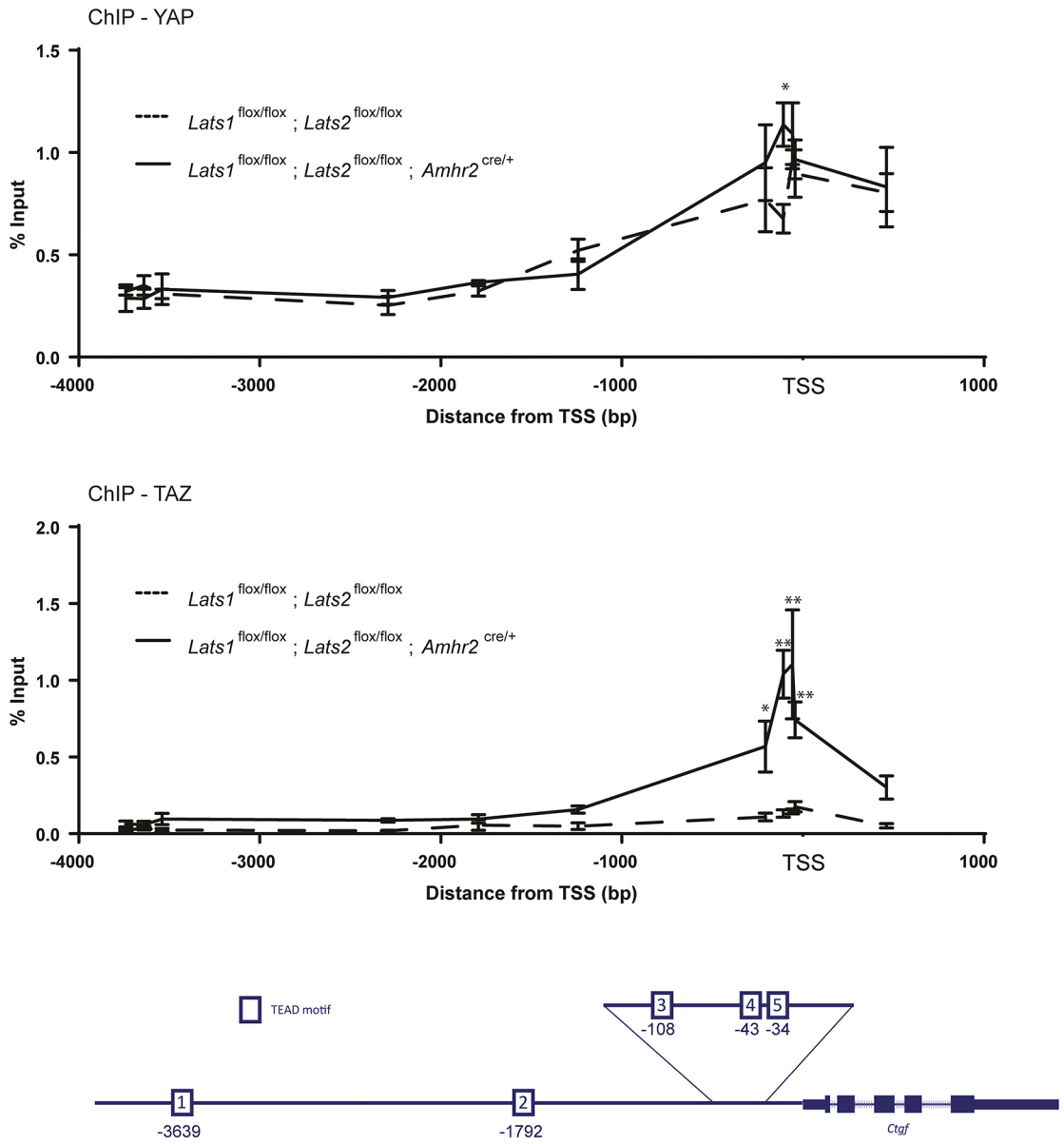

Fig. 7. Chromatin immunoprecipitation analyses. ChIP-qPCR was performed using uteri from P1 *Lats1*$^{flox/flox}$; *Lats2*$^{flox/flox}$; *Amhr2*$^{cre/+}$ (mutant) mice or *Lats1*$^{flox/flox}$; *Lats2*$^{flox/flox}$ (control) mice to evaluate the enrichment of YAP and TAZ on the *Ctgf* promoter. *n*=4 biological replicates/genotype. Data are presented as mean±s.e.m. **P*<0.01, ***P*<0.0001 (compared with controls, two-way ANOVA). Schematic below the graphs illustrates the expected localization of the TEAD binding motifs on the Ctgf promoter (in bp distance from the transcriptional start site).

pluripotency, apparently along with the capacity to become endometrial stromal and myometrial smooth muscle cells. That the inactivation of *Lats1* or *Lats2* alone in Müllerian mesenchyme cells has no discernable effect shows that *Lats1* and *Lats2* are entirely functionally redundant in this context. Together, these results define a key function of Hippo signaling in the developing female reproductive tract, and provide novel insight into the biology of Müllerian mesenchyme cells.

Induction of the myofibroblast cell fate in *Lats1*$^{flox/flox}$; *Lats2*$^{flox/flox}$; *Amhr2*$^{cre/+}$ mice involves YAP/TAZ-dependent induction of *Ctgf*, but not CTNNB1

As Hippo is a known regulator of WNT signaling, we originally expected that the inactivation of Hippo signaling in the *Lats1*$^{flox/flox}$; *Lats2*$^{flox/flox}$; *Amhr2*$^{cre/+}$ model would result in the stabilization of CTNNB1 in Müllerian mesenchyme cells. However, we were unable to find any evidence of enhanced CTNNB1 expression. Consistent with this, the phenotypic changes observed in the reproductive tracts of *Lats1*$^{flox/flox}$; *Lats2*$^{flox/flox}$; *Amhr2*$^{cre/+}$ mice appeared completely unrelated to those in any previously reported mouse models in which WNT signaling was altered in the Müllerian duct (Dunlap et al., 2011; Farah et al., 2017; Franco et al., 2011; Mericskay et al., 2004; Prunskaite-Hyyrylainen et al., 2016; St-Jean et al., 2019; Vainio et al., 1999). Inactivation of Hippo in *Lats1*$^{flox/flox}$; *Lats2*$^{flox/flox}$; *Amhr2*$^{cre/+}$ mice did, however, clearly result in the activation of the canonical Hippo effectors YAP and TAZ, as shown by their increased expression, along with that of their transcriptional target genes. WNT and Hippo signaling may therefore work independently of each other in Müllerian mesenchyme cells. Moreover, YAP/TAZ can even antagonize CTNNB1 signaling in certain contexts (Park et al., 2015), although we were unable to determine whether this occurs in the *Lats1*$^{flox/flox}$; *Lats2*$^{flox/flox}$; *Amhr2*$^{cre/+}$ model.

Development (2019) 146, dev180430. doi:10.1242/dev.180430

CTGF has been previously described as a key driver of myofibroblast activation and differentiation (Garrett et al., 2004; Grotendorst et al., 2004; Klingberg et al., 2013; Lipson et al., 2012; Sakai et al., 2017; Yang et al., 2015). Furthermore, it is thought to be a direct transcriptional target of the Hippo pathway (Di Benedetto et al., 2016; Zhao et al., 2008), and is among the most highly overexpressed genes in the Müllerian ducts of *Lats1*$^{flox/flox}$; *Lats2*$^{flox/flox}$; *Amhr2*$^{cre/+}$ mice. Together, these observations suggested that the induction of *Ctgf* could be a key mechanism whereby loss of Hippo signaling causes Müllerian mesenchyme cells to commit to the myofibroblast fate in the *Lats1*$^{flox/flox}$; *Lats2*$^{flox/flox}$; *Amhr2*$^{cre/+}$ model, and prompted us to investigate the underlying mechanism. We were able to show an enhanced recruitment of YAP and TAZ to the proximal promoter of *Ctgf* in a region that includes a cluster of three consensus TEAD binding motifs, strongly suggesting that overexpressed YAP and TAZ induce *Ctgf* transcription through direct association with its promoter. This does not, however, exclude the possibility that additional mechanism(s) may be involved. For instance, *Ctgf* expression can also be regulated by TGFβ signaling via the SMAD2/3/4 pathway (Liu et al., 2013b; Parada et al., 2013) in contexts such as tissue repair and fibrosis (Lipson et al., 2012; Rachfal and Brigstock, 2003; Sakai et al., 2017; Tian et al., 2012). Several reports have shown that YAP/TAZ interact with SMAD complexes following TGFβ stimulation, and that this interaction serves to regulate both SMAD2/3/4 transcriptional activity and subcellular localization (Attisano and Wrana, 2013; Grannas et al., 2015; Mauviel et al., 2012; Szeto et al., 2016). It is therefore possible that YAP/TAZ modulation of the TGFβ pathway contributes to driving *Ctgf* overexpression in the *Lats1*$^{flox/flox}$; *Lats2*$^{flox/flox}$; *Amhr2*$^{cre/+}$ model. Further experiments will be required to test the latter hypothesis, as well as to determine the relative role of CTGF in driving the phenotypic changes observed in *Lats1*$^{flox/flox}$; *Lats2*$^{flox/flox}$; *Amhr2*$^{cre/+}$ mice.

Persistence of Müllerian structures in male *Lats1*$^{flox/flox}$; *Lats2*$^{flox/flox}$; *Amhr2*$^{cre/+}$ mice

Male reproductive tract defects were not expected in the *Lats1*$^{flox/flox}$; *Lats2*$^{flox/flox}$; *Amhr2*$^{cre/+}$ model, given the specificity of the *Amhr2*^{cre} allele for the Müllerian duct. Although the exact mechanism underlying the development of these defects remains unclear, it can be surmised that loss of *Lats1* and *Lats2* occurred in the Müllerian ducts of male mice prior to the AMH signal that would have initiated their degradation. Our microarray data showed that *Amhr2* expression is dramatically downregulated in the Müllerian ducts in *Lats1*$^{flox/flox}$; *Lats2*$^{flox/flox}$; *Amhr2*$^{cre/+}$ female mice, suggesting that loss of *Lats1* and *Lats2* could result in rapid loss of AMHR2 and consequential insensitivity to AMH. Once the Müllerian mesenchyme cells were committed to the myofibroblast fate, they appeared to interfere mechanically with the coiling and development of the epididymides and deferent ducts, and caused the testes to fail to descend, leading to pathological secondary changes in the testes as well. Some of the changes observed in the testes of *Lats1*$^{flox/flox}$; *Lats2*$^{flox/flox}$; *Amhr2*$^{cre/+}$ mice may also have been due to loss of *Lats1/2* expression in Leydig and/or Sertoli cells, as the *Amhr2*^{cre} allele has previously been shown to drive some level of Cre expression in both cell types (Boyer et al., 2008; Jeyasuria et al., 2004). However, it was impossible to unambiguously attribute phenotypic changes specifically to conditional gene inactivation in testicular cells owing to the confounding factor of cryptorchidism.

Lats1 and *Lats2* may be dispensable in endometrial stromal cells following cell fate determination

A small number of studies have suggested that YAP/TAZ may play a role in the adult uterus in processes such as decidualization and implantation (Chen et al., 2017; Strakova et al., 2010). This prompted us to determine whether the loss of Hippo signaling in endometrial stromal cells would affect their ability to decidualize. We found that loss of *Lats1/2* had no effect on decidualization in cultured endometrial stromal cells. Although this suggests that Hippo signaling is dispensable in this context, it does not necessarily indicate that YAP and TAZ do not play a role. At most, it suggests that YAP and TAZ overexpression does not inhibit decidualization in the short term. Further experiments targeting Hippo pathway effectors including *Yap* and *Taz in vivo* will be required to make a definitive conclusion. Our findings indicate that loss of *Lats1/2* in fully differentiated endometrial stromal cells does not cause any apparent loss of function or cause them to become myofibroblasts, unlike what occurs in their Müllerian mesenchyme precursors. For this reason, inactivation of Hippo effectors *in vivo* to study their roles in decidualization will likely require a strategy that avoids targeting the uterine stroma at developmental stages prior to the commitment of mesenchyme cells to the stromal cell fate.

In summary, we report here a previously unsuspected role of the Hippo pathway in the development of the female reproductive tract. *Lats1/2* activity was found to be necessary to preserve the multipotency of Müllerian mesenchyme cells and prevent them from committing to the myofibroblast cell fate. Further studies will be required to better define how Hippo signaling is regulated and acts throughout reproductive tract development, as well as its potential roles in reproductive physiology.

MATERIALS AND METHODS

Animal models and fertility trials

The *Lats1*$^{tm1.1Jfm}$ (referred to herein as *Lats1*^{flox}) and *Lats2*$^{tm1.1Jfm}$ (referred to herein as *Lats2*^{flox}) strains were obtained from Randy L. Johnson (M.D. Anderson Cancer Center, Houston, TX, USA). The *Amhr2*$^{tm3(cre)Bhr}$ (referred to herein as *Amhr2*^{cre}) strain was obtained from Richard R. Behringer (M.D. Anderson Cancer Center). *Lats1*^{flox}, *Lats2*^{flox} and *Amhr2*^{cre} strains were crossed in order to obtain the *Lats1*, *Lats2* and *Lats1/2* conditional knockout genotypes described in the text. All strains were maintained on a C57BL/6J genetic background. Genotyping analyses were performed by PCR on DNA obtained from tail biopsies as previously described (Heallen et al., 2011; Tsoi et al., 2019).

To assess fertility in *Lats1*$^{flox/flox}$; *Amhr2*$^{cre/+}$, *Lats2*$^{flox/flox}$; *Amhr2*$^{cre/+}$ and *Lats1*$^{flox/flox}$; *Lats2*$^{flox/flox}$; *Amhr2*$^{cre/+}$ mice, 8-week-old females were housed with 8-week-old wild-type (C57BL/6J) males and monitored daily for litters. Litter sizes were recorded at birth. The males were removed after 6 months and the experiment was terminated 22 days later to allow for the birth of a final litter. Seven 8-week-old *Lats1*$^{flox/flox}$; *Lats2*$^{flox/flox}$; *Amhr2*$^{cre/+}$ males were similarly housed with females for 2 months. Of these, five failed to sire pups, one sired a litter of four pups, and another sired three litters of one, four and one pup, respectively.

Morphological and histological evaluation of Müllerian ducts and uteri

Lats1$^{flox/flox}$; *Lats2*$^{flox/flox}$ (control) and *Lats1*$^{flox/flox}$; *Lats2*$^{flox/flox}$; *Amhr2*$^{cre/+}$ embryos and mice were obtained at E14.5, E17.5, E19.5, postnatal day (P)1, P21 and 2-4 months (adult) of age. For E14.5, E17.5 and E19.5 embryos, *Lats1*$^{flox/flox}$; *Lats2*$^{flox/flox}$ adult females were crossed with either *Lats1*$^{flox/+}$; *Lats2*$^{flox/flox}$; *Amhr2*$^{cre/+}$ or *Lats1*$^{flox/flox}$; *Lats2*$^{flox/+}$; *Amhr2*$^{cre/+}$ males (as conditional knockout males were infertile), and observed every morning for the presence of a vaginal plug (defined as E0.5). Gravid uteri were dissected to collect the embryos, tail biopsies taken from each embryo for genotype analyses, and the whole embryos fixed for 24 h in 4% paraformaldehyde (PFA) prior to paraffin embedding. A subset of E17.5

Development (2019) 146, dev180430. doi:10.1242/dev.180430

and E19.5 embryos was dissected to isolate the Müllerian ducts prior to fixing (PFA, 4 h) and embedding. Reproductive tracts from P1, P21 and adult mice uteri were collected, fixed in 10% neutral buffered formalin and paraffin embedded. Sections of whole embryos, Müllerian ducts and reproductive tracts were prepared at a thickness of 3 µm and stained either with Hematoxylin and Eosin-Phloxine (HE), Hematoxylin-Eosin-Phloxine-Saffron (HEPS), or Picrosirius Red. For transmission electron microscopy, uteri from P1 mice were collected and fixed in 2.5% glutaraldehyde in sodium cacodylate buffer. Processing of the tissue and transmission electron microscopy analyses were performed by the Facility for Electron Microscopy Research (FEMR) at McGill University.

RT-qPCR analyses and DNA microarray

Müllerian ducts (E17.5) and uteri (P1) were flash frozen in liquid nitrogen and stored at −70°C prior to RNA extraction. Total RNA was extracted using the Qiagen RNeasy mini kit according to the manufacturer's instructions. RNA quantity and quality was assessed using a NanoDrop-1000 spectrophotometer (Thermo Fisher Scientific). RNA was reverse-transcribed using the SuperScript Vilo cDNA Synthesis Kit (Invitrogen) following the manufacturer's instructions. Real-time PCR reactions were run using a CFX96 Real-Time System/C1000 Touch thermal cycler (Bio-Rad) and Universal SsoAdvanced SYBR Green Supermix (Bio-Rad). PCR reactions consisted of 2.3 µl of H_2O, 6 pmol of each forward and reverse gene-specific primer, and 7.5 µl of SYBR Green Supermix. Standard curves were generated using serial dilutions of cDNA, and amplification efficiency (E) values were obtained using the slope of the log-linear phase derived from the formula E=e(1/slope). Only primer pairs with efficiency values between 1.8 and 2.2 were used. The thermal cycling program to amplify transcripts typically consisted of 3 min at 95°C, followed by 40 cycles of 15 s at 95°C, 30 s at 60°C and 30 s at 72°C. To quantify relative gene expression, the cycle threshold (Ct) values for each transcript were compared with that of *Rpl19*, according to the ratio $R=(E^{Ct\ Rpl19}/E^{Ct\ target})$. MIQE guidelines were followed throughout. Primer sequences are listed in Table S3.

Total RNA from E17.5 Müllerian ducts (n=3 per group) was submitted to the McGill University and Génome Québec Innovation Centre (Montreal, Quebec, Canada) for microarray analysis using the Affymetrix Clariom S Mouse assay. Results were analyzed using Transcriptome Analysis Console software (TAC 4.0) (Thermo Fisher Scientific). Thresholds used for P-value and fold change were 0.05 and ±2, respectively. Further analyses were performed using the Metascape gene annotation and analysis resource (http://metascape.org) (Zhou et al., 2019).

In vitro stromal cell culture and decidualization assessment

Female *Lats1*$^{flox/flox}$; *Lats2*$^{flox/flox}$ mice ranging from 8 to 12 weeks of age were injected daily with estradiol (Sigma-Aldrich) (100 ng, subcutaneously) for 3 days prior to endometrial stromal and epithelial cell isolation and culture. All steps of cell purification, culture and *in vitro* decidualization were performed essentially as described by De Clercq et al. (2017). Freshly isolated stromal cells were incubated overnight to permit attachment to the cell culture plates, and subsequently infected with Ad-Cre or Ad-eGFP (Vector development laboratory, Baylor College of Medicine, Houston, TX, USA) at a multiplicity of infection of approximately 50 for 24 h. Following washes, stromal cells we co-cultured with epithelial cells grown in ThinCert cell culture inserts (Greiner Bio-One International) such that the stromal and epithelial cells remained separate but were able to communicate via a semi-permeable membrane. Following medroxyprogesterone/cAMP (Sigma-Aldrich) treatment for 48-72 h, *Lats1*, *Lats2* and *Prl8a2* mRNA levels were assessed by RT-qPCR as described above. Similar experiments were also performed without co-culturing with epithelial cells and *Acta2*, *Cnn1*, *Cald1* mRNA levels were assessed by RT-qPCR as described above.

Immunohistochemistry and proliferation assay

Immunohistochemical (IHC) analyses were performed either on PFA (E17.5) or formalin (P1)-fixed, paraffin-embedded Müllerian ducts and uteri were sectioned at a thickness of 3 µm. Following deparaffinization, rehydration, sodium citrate heat-mediated antigen retrieval and peroxidase block, primary antibodies were diluted in Signal Stain Antibody Diluent (8112; Cell Signaling Technology) and incubated overnight at 4°C. Antibodies used include LATS1 at 1:100-1:500 (SC-28223; Santa Cruz Biotechnology), LATS2 at 1:600 (orb6306; Biorbyt), YAP at 1:200 (4912S; Cell Signaling Technology), TAZ at 1:500 (4883S; Cell Signaling Technology), pYAP at 1:100 (13008S; Cell Signaling Technology), vimentin at 1:100 (5741S; Cell Signaling Technology), PTGS2 at 1:300 (12282S; Cell Signaling Technology), total CTNNB1 at 1:100 (D10A8; Cell Signaling Technology), active CTNNB1 at 1:600 (D13A1; Cell Signaling Technology), pre-diluted CK19 (ab961; Abcam), PAX8 at 1:1000 (10336-1-AP; Proteintech), inhibin at 1:100 (M3609; Dako), calretinin at 1:50 (MA5-14540; Thermo Fisher Scientific), WT1 at 1:100 (M3561; Dako), CK5 at 1:200 (MA5-17057; Thermo Fisher Scientific), PAX2 at 1:100 (ab79389; Abcam) and Ki67 at 1:250 (ab16667, Abcam). Detection was performed with the Vectastain Elite ABC HRP Kit (Vector Laboratories, PK-6101) and the 3,3′-diaminobenzidine peroxidase substrate kit (Vector Laboratories, SK-4100). Slides were counterstained with Hematoxylin prior to mounting. IHC for smooth muscle actin was carried out using a LabVision autostainer (Thermo Fisher Scientific), with the primary antibody (MU128-UC; Biogenex) diluted at 1:100 and incubated for 1 h at room temperature. Detection was performed using Kit Envision System AEC Mouse (K4005; Agilent Technologies). To assay proliferation, BrdU (B5002; Sigma-Aldrich) was dissolved as per manufacturer instructions (10 mg/ml in 0.9% saline) and injected in gravid mice at E17.5 (100 mg/kg, intraperitoneally). Mice were sacrificed 3 h post-injection. Embryos were collected, fixed for 24 h in PFA, paraffin embedded and 3-µm-thick sections prepared. Immunohistochemistry was then performed using the M.O.M. Kit (PK-2200; Vector Laboratories) with the BrdU primary antibody (M0744; Agilent Technologies) incubated at the manufacturer's suggested dilution for 1 h at room temperature. Detection was then performed using the Vectastain Elite ABC kit as described above.

Chromatin immunoprecipitation

Chromatin immunoprecipitation (ChIP) experiments were performed using frozen uteri (P1) as previously described (Svotelis et al., 2009), with the exception of using magnetic dynabeads (Thermo Fisher Scientific, 10002D) for immunoprecipitation. Briefly, samples (n=4 biological replicates per group, 3 pooled uteri per replicate) were crosslinked with 1.1% formaldehyde for 10 min at 37°C with agitation. The crosslinking reaction was stopped by addition of glycine (0.125 M for 10 min at 37°C with agitation) followed by two washes with cold PBS. Crosslinked uteri were ground in SDS lysis buffer using a mortar and pestle prior to sonication. Immunoprecipitation was carried out using 1 µg of TAZ antibody (4883S; Cell Signaling Technology), 1 µg of YAP antibody (NB110-58358; Novus Biologicals), or no antibody as background control. qPCR assays were performed on immunoprecipitated DNA and quantified using a standard curve derived from total (i.e. input) DNA. Background signal was removed by subtracting the signal obtained in 'no antibody' controls from that obtained in samples immunoprecipitated with the YAP or TAZ antibodies. Primers used for the amplification of specific regions of the *Ctgf* promoter are listed in Table S4. Background results were brought to 0.1% of input for TAZ enrichment and 0.1% of input for YAP enrichment.

Statistical analysis

Analyses were performed using GraphPad Prism 6 software (GraphPad Software). All data were subjected to the F test to determine the equality of variances. Data were transformed to logarithms if they were not normally distributed. Statistical significance was determined using unpaired Student's t-test or ANOVA, with $P<0.05$ considered significant. Data are presented as means±s.e.m.

Acknowledgements

The authors thank Ms Nancy Veilleux and Ms Jacinthe Cardin for assistance with sectioning of processed tissues and Ms Jeannie Mui for assistance during the preparation and evaluation of tissue for transmission electron microscopy.

Competing interests

The authors declare no competing or financial interests.

Author contributions

Conceptualization: G.S.-J., M.T., A.A., A.L., C.R., M.M., B.D., N.G., A.B., B.V., D.B.; Methodology: G.S.-J., M.T., A.A., A.L., C.R., M.M., B.D., N.G., A.B., B.V., D.B.; Formal analysis: G.S.-J., M.T., B.D., I.M., R.K., M.P., N.G., A.B., B.V., D.B.; Investigation: G.S.-J., M.T., A.A., A.L., C.R., M.M., B.D., D.B.; Resources: D.B.; Data curation: G.S.-J., D.B.; Writing - original draft: G.S.-J., D.B.; Writing - review & editing: G.S.-J., M.T., M.M., B.V., D.B.; Visualization: D.B.; Supervision: D.B.; Project administration: D.B.; Funding acquisition: D.B.

Funding

This work was supported by a Canadian Institutes of Health Research (CIHR) project grant (MOP-142445 to D.B.). G.S.-J. was supported by a doctoral research award from the Fonds de Recherche du Québec - Santé (FRQS).

Data availability

Microarray data have been deposited in the GEO database under accession number GSE135855.

Supplementary information

Supplementary information available online at
http://dev.biologists.org/lookup/doi/10.1242/dev.180430.supplemental

References

Arango, N. A., Kobayashi, A., Wang, Y., Jamin, S. P., Lee, H.-H., Orvis, G. D. and Behringer, R. R. (2008). A mesenchymal perspective of Mullerian duct differentiation and regression in Amhr2-lacZ mice. *Mol. Reprod. Dev.* **75**, 1154-1162. doi:10.1002/mrd.20858

Attisano, L. and Wrana, J. L. (2013). Signal integration in TGF-β, WNT, and Hippo pathways. *F1000Prime Reports* **5**, 17. doi:10.12703/P5-17

Azzolin, L., Panciera, T., Soligo, S., Enzo, E., Bicciato, S., Dupont, S., Bresolin, S., Frasson, C., Basso, G., Guzzardo, V. et al. (2014). YAP/TAZ incorporation in the beta-catenin destruction complex orchestrates the Wnt response. *Cell* **158**, 157-170. doi:10.1016/j.cell.2014.06.013

Baarends, W. M., van Helmond, M. J., Post, M., van der Schoot, P. J., Hoogerbrugge, J. W., de Winter, J. P., Uilenbroek, J. T., Karels, B., Wilming, L. G. and Meijers, J. H. (1994). A novel member of the transmembrane serine/threonine kinase receptor family is specifically expressed in the gonads and in mesenchymal cells adjacent to the mullerian duct. *Development* **120**, 189-197.

Bao, X. M., He, Q., Wang, Y., Huang, Z. H. and Yuan, Z. Q. (2017). The roles and mechanisms of the Hippo/YAP signaling pathway in the nervous system. *Yi Chuan* **39**, 630-641. doi:10.16288/j.yczz.17-069

Boyer, A., Hermo, L., Paquet, M., Robaire, B. and Boerboom, D. (2008). Seminiferous tubule degeneration and infertility in mice with sustained activation of WNT/CTNNB1 signaling in sertoli cells. *Biol. Reprod.* **79**, 475-485. doi:10.1095/biolreprod.108.068627

Chen, H., Song, Y., Yang, S., Fu, J., Feng, X. and Huang, W. (2017). YAP mediates human decidualization of the uterine endometrial stromal cells. *Placenta* **53**, 30-35. doi:10.1016/j.placenta.2017.03.013

De Clercq, K., Hennes, A. and Vriens, J. (2017). Isolation of mouse endometrial epithelial and stromal cells for in vitro decidualization. *J. Vis. Exp.* **121**, 55168. doi:10.3791/55168

Deutscher, E. and Hung-Chang Yao, H. (2007). Essential roles of mesenchyme-derived beta-catenin in mouse Mullerian duct morphogenesis. *Dev. Biol.* **307**, 227-236. doi:10.1016/j.ydbio.2007.04.036

Di Benedetto, A., Mottolese, M., Sperati, F., Ercolani, C., Di Lauro, L., Pizzuti, L., Vici, P., Terrenato, I., Sperduti, I., Shaaban, A. M. et al. (2016). The Hippo transducers TAZ/YAP and their target CTGF in male breast cancer. *Oncotarget* **7**, 43188-43198. doi:10.18632/oncotarget.9668

Dunlap, K. A., Filant, J., Hayashi, K., Rucker, E. B., III, Song, G., Deng, J. M., Behringer, R. R., DeMayo, F. J., Lydon, J., Jeong, J. W. et al. (2011). Postnatal deletion of Wnt7a inhibits uterine gland morphogenesis and compromises adult fertility in mice. *Biol. Reprod.* **85**, 386-396. doi:10.1095/biolreprod.111.091769

Elbjeirami, W. M., Truong, L. D., Tawil, A., Wang, W., Dawson, S., Lan, H. Y., Zhang, P., Garcia, G. E. and Wayne Smith, C. (2010). Early differential expression of oncostatin M in obstructive nephropathy. *J. Interferon Cytokine Res.* **30**, 513-523. doi:10.1089/jir.2009.0105

Eyden, B. (2008). The myofibroblast: phenotypic characterization as a prerequisite to understanding its functions in translational medicine. *J. Cell. Mol. Med.* **12**, 22-37. doi:10.1111/j.1582-4934.2007.00213.x

Farah, O., Biechele, S., Rossant, J. and Dufort, D. (2017). Porcupine-dependent Wnt signaling controls stromal proliferation and endometrial gland maintenance through the action of distinct WNTs. *Dev. Biol.* **422**, 58-69. doi:10.1016/j.ydbio.2016.11.023

Franco, H. L., Dai, D., Lee, K. Y., Rubel, C. A., Roop, D., Boerboom, D., Jeong, J.-W., Lydon, J. P., Bagchi, I. C., Bagchi, M. K. et al. (2011). WNT4 is a key regulator of normal postnatal uterine development and progesterone signaling during embryo implantation and decidualization in the mouse. *FASEB J.* **25**, 1176-1187. doi:10.1096/fj.10-175349

Garrett, Q., Khaw, P. T., Blalock, T. D., Schultz, G. S., Grotendorst, G. R. and Daniels, J. T. (2004). Involvement of CTGF in TGF-beta1-stimulation of myofibroblast differentiation and collagen matrix contraction in the presence of mechanical stress. *Invest. Ophthalmol. Vis. Sci.* **45**, 1109-1116. doi:10.1167/iovs.03-0660

Gerarduzzi, C. and Di Battista, J. A. (2017). Myofibroblast repair mechanisms post-inflammatory response: a fibrotic perspective. *Inflamm. Res.* **66**, 451-465. doi:10.1007/s00011-016-1019-x

Gomez, I. G., Roach, A. M., Nakagawa, N., Amatucci, A., Johnson, B. G., Dunn, K., Kelly, M. C., Karaca, G., Zheng, T. S., Szak, S. et al. (2016). TWEAK-Fn14 signaling activates myofibroblasts to drive progression of fibrotic kidney disease. *J. Am. Soc. Nephrol.* **27**, 3639-3652. doi:10.1681/ASN.2015111227

Grannas, K., Arngården, L., Lönn, P., Mazurkiewicz, M., Blokzijl, A., Zieba, A. and Söderberg, O. (2015). Crosstalk between hippo and TGFbeta: subcellular localization of YAP/TAZ/Smad complexes. *J. Mol. Biol.* **427**, 3407-3415. doi:10.1016/j.jmb.2015.04.015

Grotendorst, G. R., Rahmanie, H. and Duncan, M. R. (2004). Combinatorial signaling pathways determine fibroblast proliferation and myofibroblast differentiation. *FASEB J.* **18**, 469-479. doi:10.1096/fj.03-0699com

Heallen, T., Zhang, M., Wang, J., Bonilla-Claudio, M., Klysik, E., Johnson, R. L. and Martin, J. F. (2011). Hippo pathway inhibits Wnt signaling to restrain cardiomyocyte proliferation and heart size. *Science* **332**, 458-461. doi:10.1126/science.1199010

Hernandez Gifford, J. A., Hunzicker-Dunn, M. E. and Nilson, J. H. (2009). Conditional deletion of beta-catenin mediated by Amhr2cre in mice causes female infertility. *Biol. Reprod.* **80**, 1282-1292. doi:10.1095/biolreprod.108.072280

Jamin, S. P., Arango, N. A., Mishina, Y., Hanks, M. C. and Behringer, R. R. (2002). Requirement of Bmpr1a for Müllerian duct regression during male sexual development. *Nat. Genet.* **32**, 408-410. doi:10.1038/ng1003

Jeyasuria, P., Ikeda, Y., Jamin, S. P., Zhao, L., De Rooij, D. G., Themmen, A. P. N., Behringer, R. R. and Parker, K. L. (2004). Cell-specific knockout of steroidogenic factor 1 reveals its essential roles in gonadal function. *Mol. Endocrinol.* **18**, 1610-1619. doi:10.1210/me.2003-0404

Klingberg, F., Hinz, B. and White, E. S. (2013). The myofibroblast matrix: implications for tissue repair and fibrosis. *J. Pathol.* **229**, 298-309. doi:10.1002/path.4104

Lee, D.-H., Park, J. O., Kim, T.-S., Kim, S.-K., Kim, T.-H., Kim, M.-C., Park, G. S., Kim, J.-H., Kuninaka, S., Olson, E. N. et al. (2016). LATS-YAP/TAZ controls lineage specification by regulating TGFbeta signaling and Hnf4alpha expression during liver development. *Nat. Commun.* **7**, 11961. doi:10.1038/ncomms11961

Lenga, Y., Koh, A., Perera, A. S., McCulloch, C. A., Sodek, J. and Zohar, R. (2008). Osteopontin expression is required for myofibroblast differentiation. *Circ. Res.* **102**, 319-327. doi:10.1161/CIRCRESAHA.107.160408

Lipson, K. E., Wong, C., Teng, Y. and Spong, S. (2012). CTGF is a central mediator of tissue remodeling and fibrosis and its inhibition can reverse the process of fibrosis. *Fibrogenesis Tissue Repair* **5**, S24. doi:10.1186/1755-1536-5-S1-S24

Liu, T., Liu, Y., Gao, H., Meng, F., Yang, S. and Lou, G. (2013a). Clinical significance of yes-associated protein overexpression in cervical carcinoma: the differential effects based on histotypes. *Int. J. Gynecol. Cancer* **23**, 735-742. doi:10.1097/IGC.0b013e31828c8619

Liu, Y., Liu, H., Meyer, C., Li, J., Nadalin, S., Königsrainer, A., Weng, H., Dooley, S. and ten Dijke, P. (2013b). Transforming growth factor-beta (TGF-beta)-mediated connective tissue growth factor (CTGF) expression in hepatic stellate cells requires Stat3 signaling activation. *J. Biol. Chem.* **288**, 30708-30719. doi:10.1074/jbc.M113.478685

Lv, X. B., Liu, C. Y., Wang, Z., Sun, Y. P., Xiong, Y., Lei, Q. Y. and Guan, K. L. (2015). PARD3 induces TAZ activation and cell growth by promoting LATS1 and PP1 interaction. *EMBO Rep.* **16**, 975-985. doi:10.15252/embr.201439951

Mauviel, A., Nallet-Staub, F. and Varelas, X. (2012). Integrating developmental signals: a Hippo in the (path)way. *Oncogene* **31**, 1743-1756. doi:10.1038/onc.2011.363

McNeill, H. and Reginensi, A. (2017). Lats1/2 regulate Yap/Taz to control nephron progenitor epithelialization and inhibit myofibroblast formation. *J. Am. Soc. Nephrol.* **28**, 852-861. doi:10.1681/ASN.2016060611

Mericskay, M., Kitajewski, J. and Sassoon, D. (2004). Wnt5a is required for proper epithelial-mesenchymal interactions in the uterus. *Development* **131**, 2061-2072. doi:10.1242/dev.01090

Miesfeld, J. B., Gestri, G., Clark, B. S., Flinn, M. A., Poole, R. J., Bader, J. R., Besharse, J. C., Wilson, S. W. and Link, B. A. (2015). Yap and Taz regulate retinal pigment epithelial cell fate. *Development* **142**, 3021-3032. doi:10.1242/dev.119008

Mifflin, R. C., Saada, J. I., Di Mari, J. F., Adegboyega, P. A., Valentich, J. D. and Powell, D. W. (2002). Regulation of COX-2 expression in human intestinal myofibroblasts: mechanisms of IL-1-mediated induction. *Am. J. Physiol. Cell Physiol.* **282**, C824-C834. doi:10.1152/ajpcell.00388.2001

Nguyen, Q., Anders, R. A., Alpini, G. and Bai, H. (2015). Yes-associated protein in the liver: regulation of hepatic development, repair, cell fate determination and tumorigenesis. *Dig. Liver Dis.* **47**, 826-835. doi:10.1016/j.dld.2015.05.011

Nightingale, J., Patel, S., Suzuki, N., Buxton, R., Takagi, K. I., Suzuki, J., Sumi, Y., Imaizumi, A., Mason, R. M. and Zhang, Z. (2004). Oncostatin M, a cytokine released by activated mononuclear cells, induces epithelial cell-myofibroblast transdifferentiation via Jak/Stat pathway activation. *J. Am. Soc. Nephrol.* **15**, 21-32. doi:10.1097/01.ASN.0000102479.92582.43

Parada, C., Li, J., Iwata, J., Suzuki, A. and Chai, Y. (2013). CTGF mediates Smad-dependent transforming growth factor β signaling to regulate mesenchymal cell proliferation during palate development. *Mol. Cell. Biol.* **33**, 3482-3493. doi:10.1128/MCB.00615-13

Park, H. W., Kim, Y. C., Yu, B., Moroishi, T., Mo, J.-S., Plouffe, S. W., Meng, Z., Lin, K. C., Yu, F.-X., Alexander, C. M. et al. (2015). Alternative Wnt signaling activates YAP/TAZ. *Cell* **162**, 780-794. doi:10.1016/j.cell.2015.07.013

Prunskaite-Hyyryläinen, R., Skovorodkin, I., Xu, Q., Miinalainen, I., Shan, J. and Vainio, S. J. (2016). Wnt4 coordinates directional cell migration and extension of the Mullerian duct essential for ontogenesis of the female reproductive tract. *Hum. Mol. Genet.* **25**, 1059-1073. doi:10.1093/hmg/ddv621

Rachfal, A. W. and Brigstock, D. R. (2003). Connective tissue growth factor (CTGF/CCN2) in hepatic fibrosis. *Hepatol. Res.* **26**, 1-9. doi:10.1016/S1386-6346(03)00115-3

Reginensi, A., Enderle, L., Gregorieff, A., Johnson, R. L., Wrana, J. L. and McNeill, H. (2016). A critical role for NF2 and the Hippo pathway in branching morphogenesis. *Nat. Commun.* **7**, 12309. doi:10.1038/ncomms12309

Roly, Z. Y., Backhouse, B., Cutting, A., Tan, T. Y., Sinclair, A. H., Ayers, K. L., Major, A. T. and Smith, C. A. (2018). The cell biology and molecular genetics of Mullerian duct development. *Wiley Interdiscip. Rev. Dev. Biol.* **7**, e310. doi:10.1002/wdev.310

Sakai, N., Nakamura, M., Lipson, K. E., Miyake, T., Kamikawa, Y., Sagara, A., Shinozaki, Y., Kitajima, S., Toyama, T., Hara, A. et al. (2017). Inhibition of CTGF ameliorates peritoneal fibrosis through suppression of fibroblast and myofibroblast accumulation and angiogenesis. *Sci. Rep.* **7**, 5392. doi:10.1038/s41598-017-05624-2

Sasaki, H. (2017). Roles and regulations of Hippo signaling during preimplantation mouse development. *Dev. Growth Differ.* **59**, 12-20. doi:10.1111/dgd.12335

Sobral, L. M., Bufalino, A., Lopes, M. A., Graner, E., Salo, T. and Coletta, R. D. (2011). Myofibroblasts in the stroma of oral cancer promote tumorigenesis via secretion of activin A. *Oral Oncol.* **47**, 840-846. doi:10.1016/j.oraloncology.2011.06.011

Song, Y., Fu, J., Zhou, M., Xiao, L., Feng, X., Chen, H. and Huang, W. (2016). Activated hippo/yes-associated protein pathway promotes cell proliferation and anti-apoptosis in endometrial stromal cells of endometriosis. *J. Clin. Endocrinol. Metab.* **101**, 1552-1561. doi:10.1210/jc.2016-1120

St-Jean, G., Boyer, A., Zamberlam, G., Godin, P., Paquet, M. and Boerboom, D. (2019). Targeted ablation of Wnt4 and Wnt5a in Mullerian duct mesenchyme impedes endometrial gland development and causes partial Mullerian agenesis. *Biol. Reprod.* **100**, 49-60. doi:10.1093/biolre/ioy160

Strakova, Z., Reed, J. and Ihnatovych, I. (2010). Human transcriptional coactivator with PDZ-binding motif (TAZ) is downregulated during decidualization. *Biol. Reprod.* **82**, 1112-1118. doi:10.1095/biolreprod.109.081844

Svotelis, A., Gévry, N. and Gaudreau, L. (2009). Chromatin Immunoprecipitation in Mammalian Cells. In *DNA-Protein Interactions. Methods in Molecular Biology (Methods and Protocols)*, Vol. 543 (ed. B. Leblanc and T. Moss), pp. 243-251. Humana Press.

Szeto, S. G., Narimatsu, M., Lu, M., He, X., Sidiqi, A. M., Tolosa, M. F., Chan, L., De Freitas, K., Bialik, J. F., Majumder, S. et al. (2016). YAP/TAZ Are Mechanoregulators of TGF-beta-Smad Signaling and Renal Fibrogenesis. *J. Am. Soc. Nephrol.* **27**, 3117-3128. doi:10.1681/ASN.2015050499

Teixeira, J., He, W. W., Shah, P. C., Morikawa, N., Lee, M. M., Catlin, E. A., Hudson, P. L., Wing, J., Maclaughlin, D. T. and Donahoe, P. K. (1996). Developmental expression of a candidate mullerian inhibiting substance type II receptor. *Endocrinology* **137**, 160-165. doi:10.1210/endo.137.1.8536608

Tian, J., Yang, F. and Liu, H. (2012). TGF-Beta and CTGF Mediated Signal Transduction Pathway and Fibrosis. In 2012 International Conference on Biomedical Engineering and Biotechnology, pp. 913-916.

Tsoi, M., Morin, M., Rico, C., Johnson, R. L., Paquet, M., Gevry, N. and Boerboom, D. (2019). Lats1 and Lats2 are required for ovarian granulosa cell fate maintenance. *FASEB J.* **33**, 10819-10832. doi:10.1096/fj.201900609R

Tsutsumi, R., Masoudi, M., Takahashi, A., Fujii, Y., Hayashi, T., Kikuchi, I., Satou, Y., Taira, M. and Hatakeyama, M. (2013). YAP and TAZ, hippo signaling targets, act as a rheostat for nuclear SHP2 function. *Dev. Cell* **26**, 658-665. doi:10.1016/j.devcel.2013.08.013

Vainio, S., Heikkilä, M., Kispert, A., Chin, N. and McMahon, A. P. (1999). Female development in mammals is regulated by Wnt-4 signalling. *Nature* **397**, 405-409. doi:10.1038/17068

Varelas, X., Miller, B. W., Sopko, R., Song, S., Gregorieff, A., Fellouse, F. A., Sakuma, R., Pawson, T., Hunziker, W., McNeill, H. et al. (2010). The Hippo pathway regulates Wnt/beta-catenin signaling. *Dev. Cell* **18**, 579-591. doi:10.1016/j.devcel.2010.03.007

Yang, Z., Sun, Z., Liu, H., Ren, Y., Shao, D., Zhang, W., Lin, J., Wolfram, J., Wang, F. and Nie, S. (2015). Connective tissue growth factor stimulates the proliferation, migration and differentiation of lung fibroblasts during paraquat-induced pulmonary fibrosis. *Mol. Med. Rep.* **12**, 1091-1097. doi:10.3892/mmr.2015.3537

Yu, F.-X., Zhao, B., Panupinthu, N., Jewell, J. L., Lian, I., Wang, L. H., Zhao, J., Yuan, H., Tumaneng, K., Li, H. et al. (2012). Regulation of the Hippo-YAP pathway by G-protein-coupled receptor signaling. *Cell* **150**, 780-791. doi:10.1016/j.cell.2012.06.037

Zhan, M., Ikeda, J. I., Wada, N., Hori, Y., Nojima, S., Tahara, S. I., Ueda, Y., Yoshino, K., Kimura, T. and Morii, E. (2016). Prognostic significance of a component of the Hippo pathway, TAZ, in human uterine endometrioid adenocarcinoma. *Oncol. Lett.* **11**, 3611-3616. doi:10.3892/ol.2016.4483

Zhao, B., Wei, X., Li, W., Udan, R. S., Yang, Q., Kim, J., Xie, J., Ikenoue, T., Yu, J., Li, L. et al. (2007). Inactivation of YAP oncoprotein by the Hippo pathway is involved in cell contact inhibition and tissue growth control. *Genes Dev.* **21**, 2747-2761. doi:10.1101/gad.1602907

Zhao, B., Ye, X., Yu, J., Li, L., Li, W., Li, S., Yu, J., Lin, J. D., Wang, C.-Y., Chinnaiyan, A. M. et al. (2008). TEAD mediates YAP-dependent gene induction and growth control. *Genes Dev.* **22**, 1962-1971. doi:10.1101/gad.1664408

Zhou, Y., Zhou, B., Pache, L., Chang, M., Khodabakhshi, A. H., Tanaseichuk, O., Benner, C. and Chanda, S. K. (2019). Metascape provides a biologist-oriented resource for the analysis of systems-level datasets. *Nat. Commun.* **10**, 1523. doi:10.1038/s41467-019-09234-6

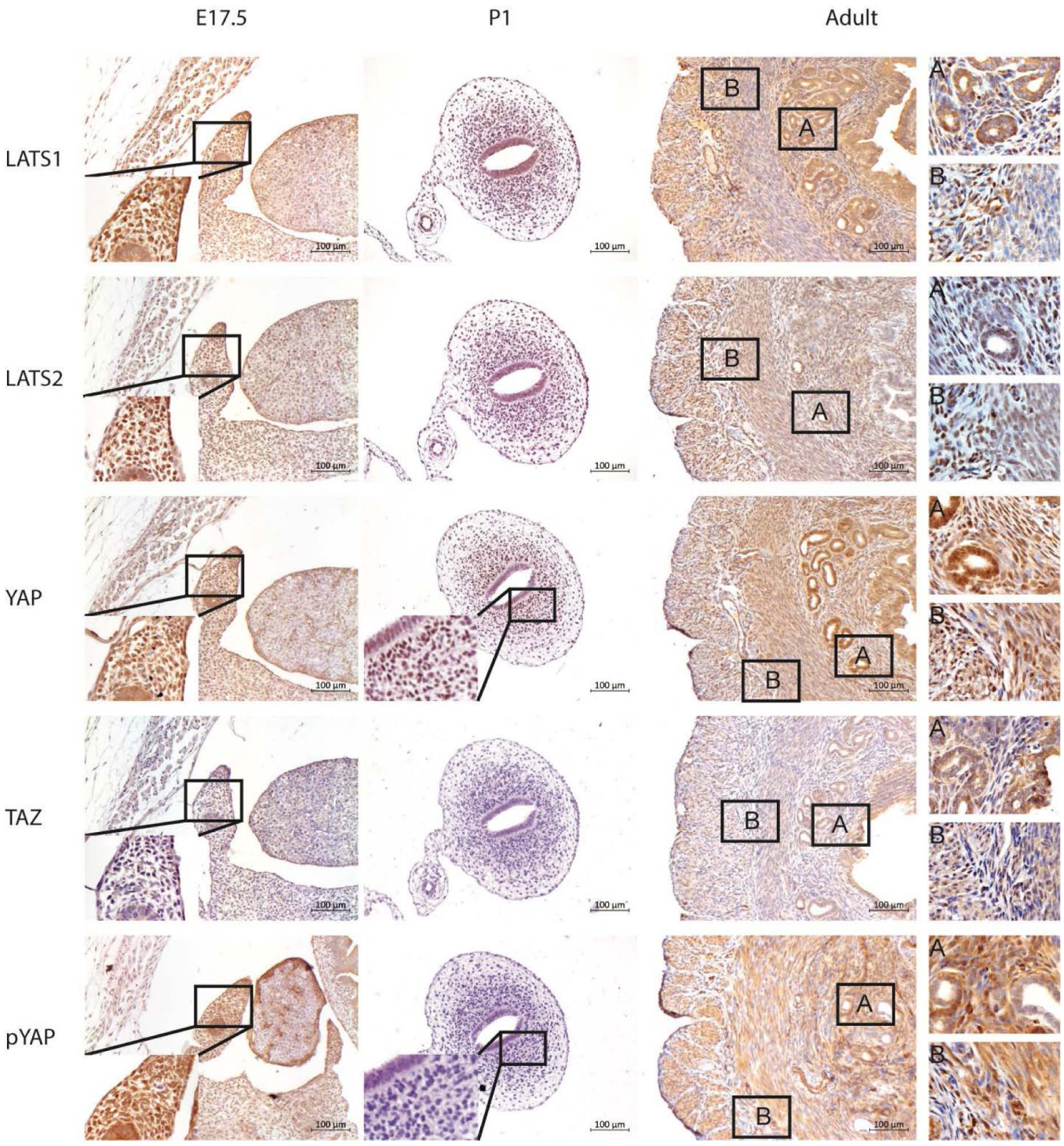

Fig. S1. Immunohistochemical analyses of Hippo core component (LATS1, LATS2, YAP, TAZ, phosphoYAP) expression during female reproductive tract development.

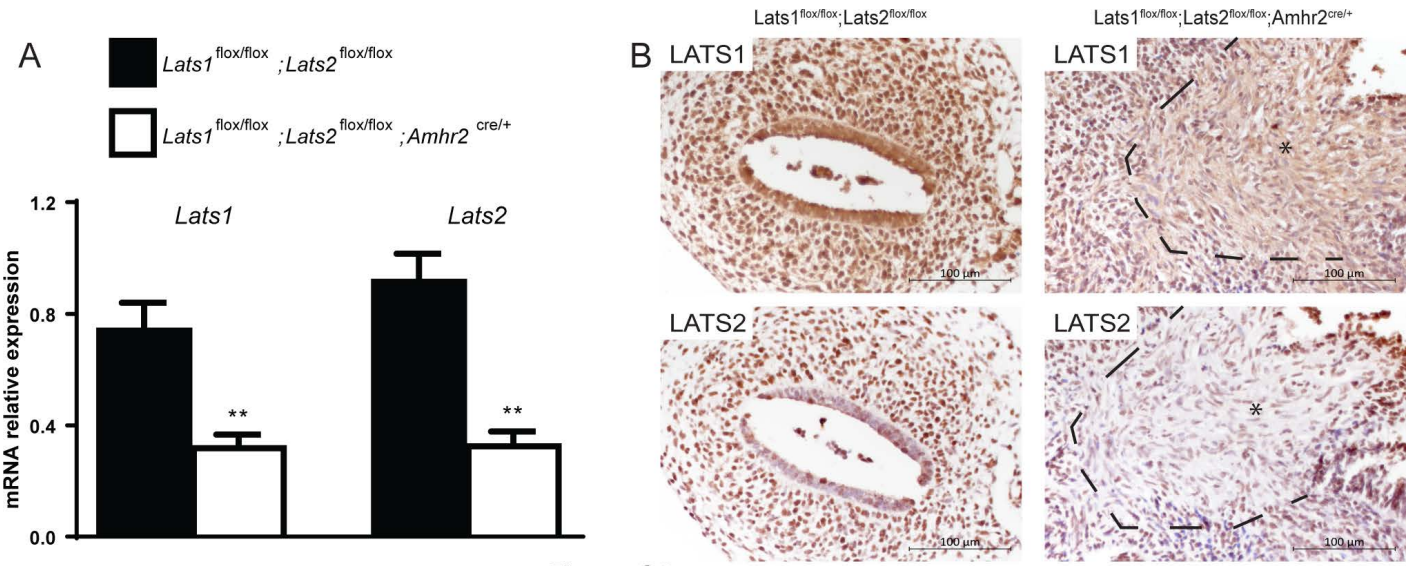

Figure S2

Fig. S2. Evaluation of knockout efficiency in the female *Lats1*$^{flox/flox}$; *Lats2*$^{flox/flox}$; *Amhr2*$^{cre/+}$ reproductive tract. (A). RT-qPCR analysis of *Lats1* and *Lats2* mRNA levels in Müllerian ducts from E17.5 mutant mice of the indicated genotypes. Data are presented as means (columns) ± s.e.m (error bars). Columns labeled with asterisks are statistically significantly different from controls (**=P<0.01, n=4, Student's t-test). (B). Immunohistochemistry analysis of LATS1 and LATS2 expression in uteri from P1 mice of the indicated genotypes. The ectopic myofibroblast cell population is delineated with a black dashed line. Apparent residual LATS1 and LATS2 staining in the myofibroblast population in the Müllerian ducts of *Lats1*$^{flox/flox}$; *Lats2*$^{flox/flox}$; *Amhr2*$^{cre/+}$ mice represents background signal.

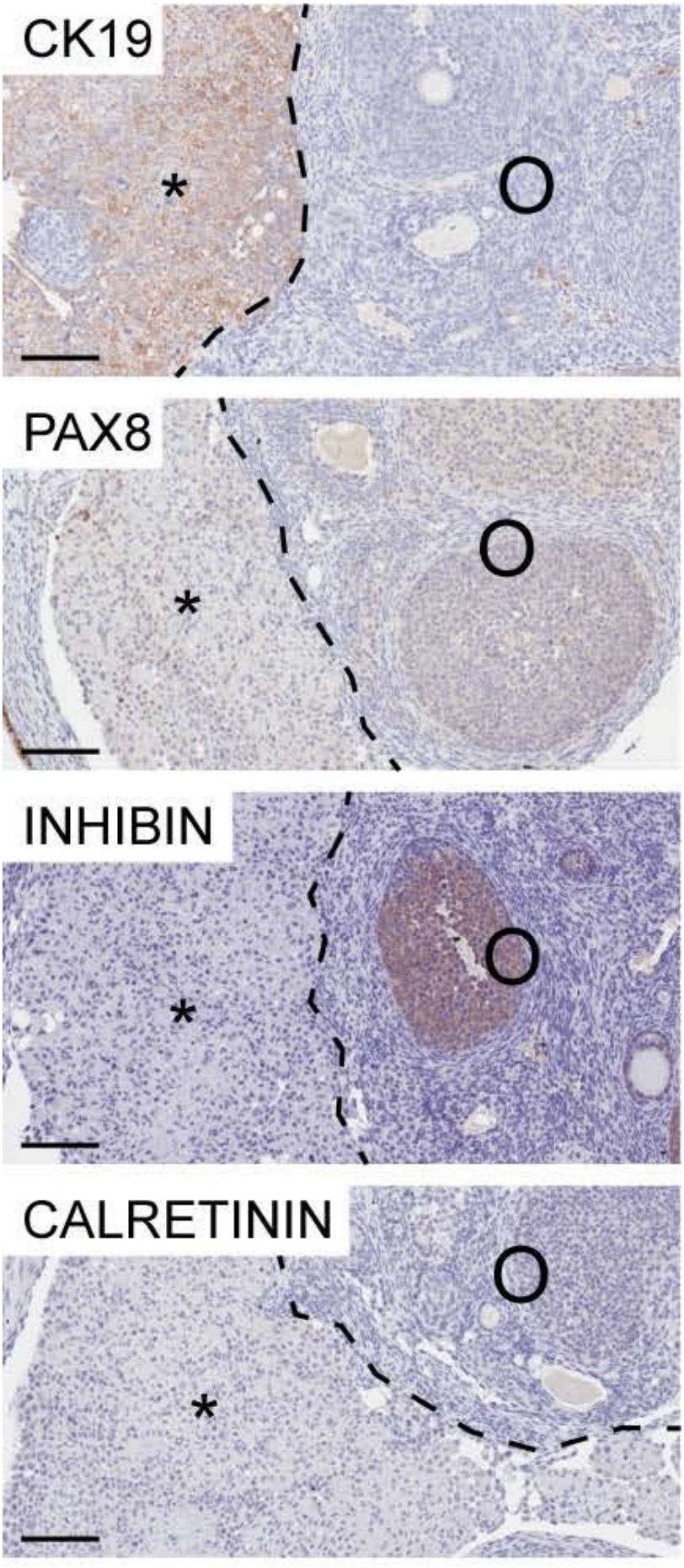

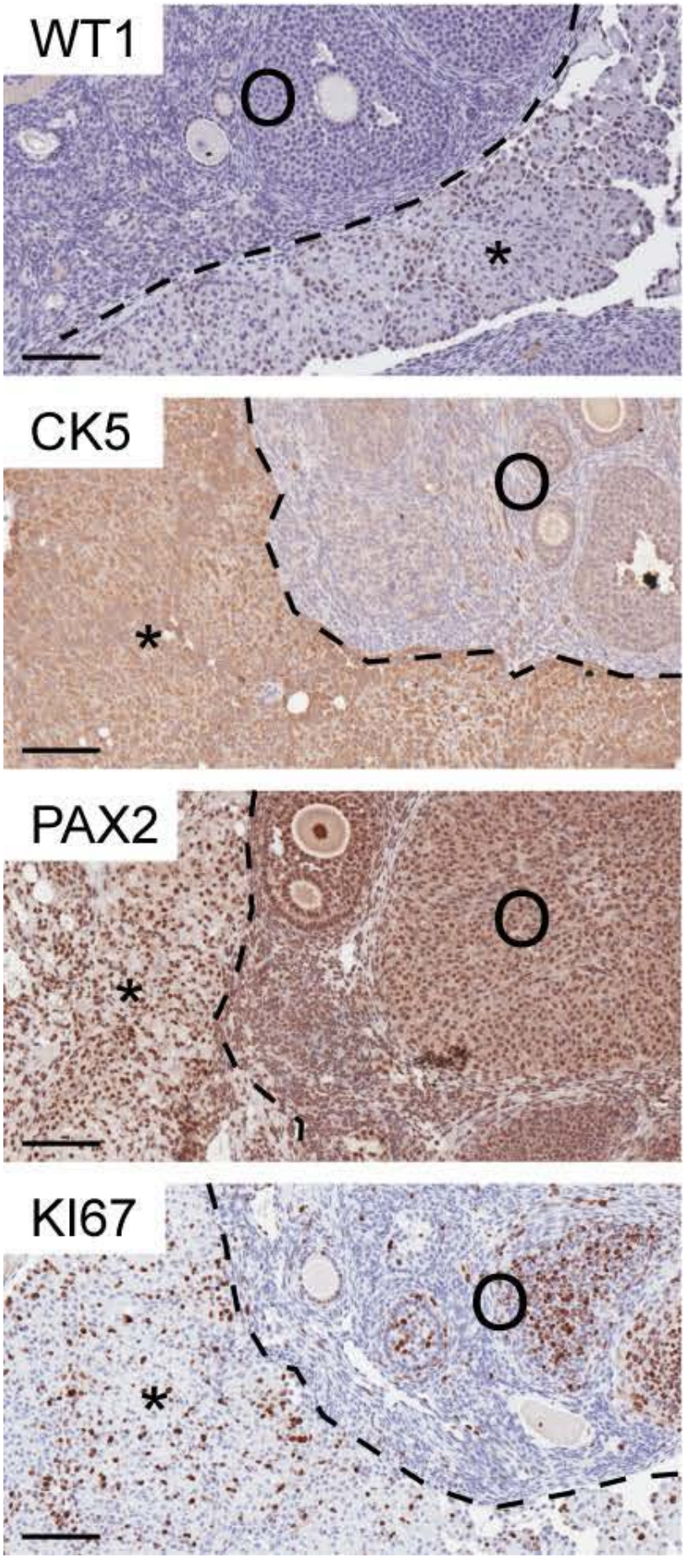

Fig. S3. Representative tumor marker immunohistochemistry photomicrographs. O = ovary, * = neoplastic tissue. Bars = 100μM.

A Biological processes associated with upregulated genes in müllerian ducts of Lats1$^{flox/flox}$; Lats2$^{flox/flox}$; Amhr2$^{cre/+}$ mice

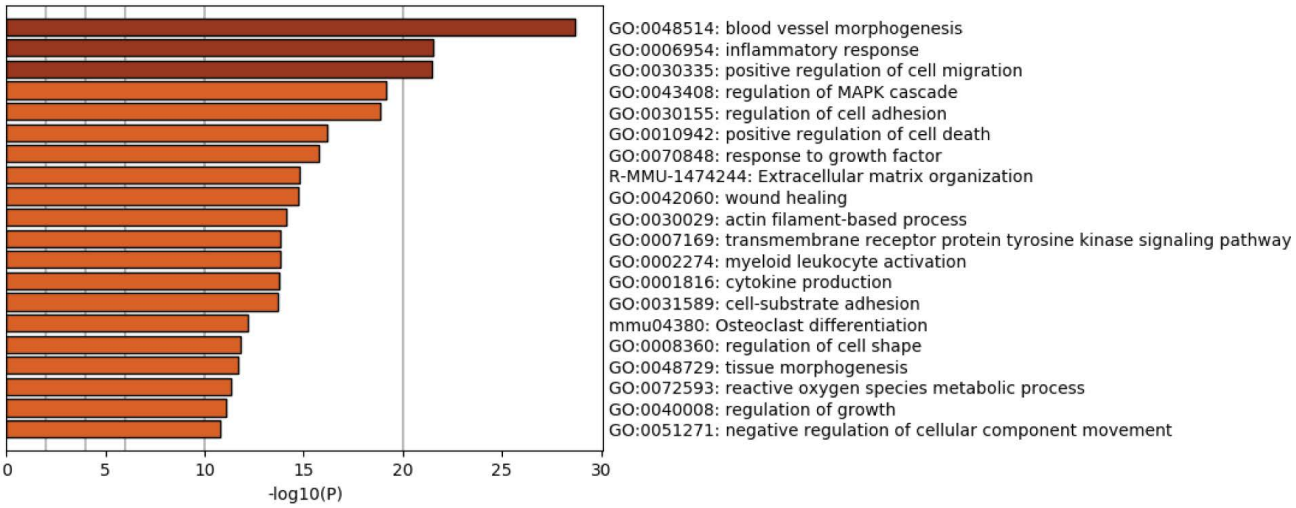

B Biological processes associated with downregulated genes in müllerian ducts of Lats1$^{flox/flox}$; Lats2$^{flox/flox}$; Amhr2$^{cre/+}$ mice

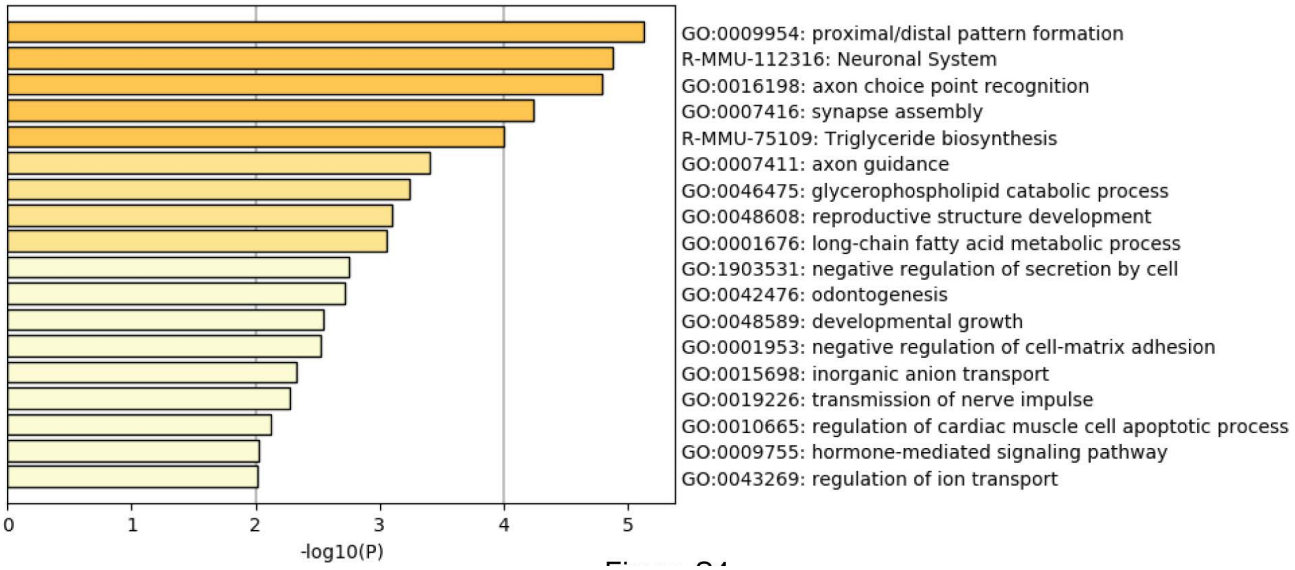

Fig. S4. Microarray gene ontogeny analysis (A). Biological processes associated with genes upregulated in the uteri of *Lats1*$^{flox/flox}$; *Lats2*$^{flox/flox}$; *Amhr2*$^{cre/+}$ mice relative to controls. (B). Biological processes associated with genes downregulated in the uteri of *Lats1*$^{flox/flox}$; *Lats2*$^{flox/flox}$; *Amhr2*$^{cre/+}$ mice relative to controls. All results were obtained using Metascape (http://metascape.org) (Zhou et al., 2019).

Table S1. Fertility trial.

Genotype	n	Total litters	Total pups	Litter size
Lats1$^{flox/flox}$;*Lats2*$^{flox/flox}$	7	7.57±0.30	67.29±5.06	8.88±0.37
Lats1$^{flox/flox}$;*Amhr2*$^{cre/+}$	6	7.86±0.14	60.86±4.90	7.75±0.46
Lats2$^{flox/flox}$;*Amhr2*$^{cre/+}$	6	7.83±0.17	55.33±4.36	7.06±0.34
Lats1$^{flox/flox}$;*Lats2*$^{flox/flox}$;*Amhr2*$^{cre/+}$	6	0.0±0.0****	0.0±0.0****	0.0±0.0****

Values are expressed as means ± SEM

**** Means are significantly different (P<0.0001)

Table S2. Tumor marker immunohistochemistry analyses.

Marker	Signal strength
CK19	++
PAX8	+
INHIBIN	-
CALRETININ	-
WT1	+/-
CK5	+++
PAX2	++
KI67	+

Table S3. qPCR primers

Gene	Forward	Reverse
Acta2	AGCCATCTTTCATTGGGATGG	CCCCTGACAGGACCTTGTTA
Cald1	GTTGCTGCCCTAGAGATAGTCA	AACCTTTGACTGTCCACCCC
Cnn1	TGCGCTTGTCTGTGTCATCT	TCTGGGCCAGCTTGTTCTTT
Ctgf	GAGGAAAACATTAAGAAGGGCAAAA	CCGCAGAACTTAGCCCTGTA
Cyr61	TTGACCAGACTGGCGCTCT	AGTTTTGCTGCAGTCCTCGT
Lats1	AGCAGCACGTAGAGAACGTC	TCTCATTTGATCCTGGGCATCT
Lats2	TGCACTGGATTCAGGTGGACTCA	GAGAATGTGCCAGGCACCTCT
Nanog	ACCTGAGCTATAAGCAGGTTAAGA	TGAATCAGACCATTGCTAGTCTTC
Oct4	CCATGTTTCTGAAGTGCCCG	ACCATACTCGAACCACATCCTTC
Prl8a2	CTCACTTCTCAGGGGCACT	AGCCATTCTCTCCTGTTTGACA
Ptgs2	CCTGAAGCCGTACACATCATTTGA	AGGCACTTGCATTGATGGTGGCT
Rpl19	CTGAAGGTCAAAGGGAATGTG	GGACAGAGTCTTGATGATCTC
Sox2	GCGGAGTGGAAACTTTTGTCC	CGGGAAGCGTGTACTTATCCTT
Spp1	CCTTGCTTGGGTTTGCAGTC	TGGTCGTAGTTAGTCCCTCAGA

Table S4. ChIP primers

Position	Forward	Reverse
-3739	CAAACATCCATGCTTCCTTCCAA	TTAAGGAGTGTGCCCTCTCACA
-3639	TCTGGCATACGCCCCCTG	TGTGTCCTAGGTTCAGTCATGT
-3539	TGCTGACAGCCCAGTGTATG	GTGGAACGTGACTCAAAGCC
-2292	CACAACGCATCTGTTTCCTG	CTCGATTTCGTTGCTCTCAGTG
-1792	GCCTCTTCTCTTTGAGGAATGCT	GTGTGAGTGGCTTGAAGTGTG
-1242	ACAACACAGGTCCTAAATGAATG	GAACTGCTACTTAGTTTCTGTAAGG
-208	CAGAACTGGCAAAGAGATTTTTAAG	TCCATATCATCTTCTCACCCCTC
-108	GCGAGCTAAAGTGTGCCAG	TTGACACTCCACATTCCTCCG
-58	GTGTCAAGGGGTCAGGATCAA	CCACCTTCCTGCCTCATCAAC
-43	TGAGTTGATGAGGCAGGAAGG	CGCCAAAGAACTGAATGGAGTC
462	GAACTGTGTACGGAGCGTGAC	CAGAAGAGGCCCTTGTGTGGG